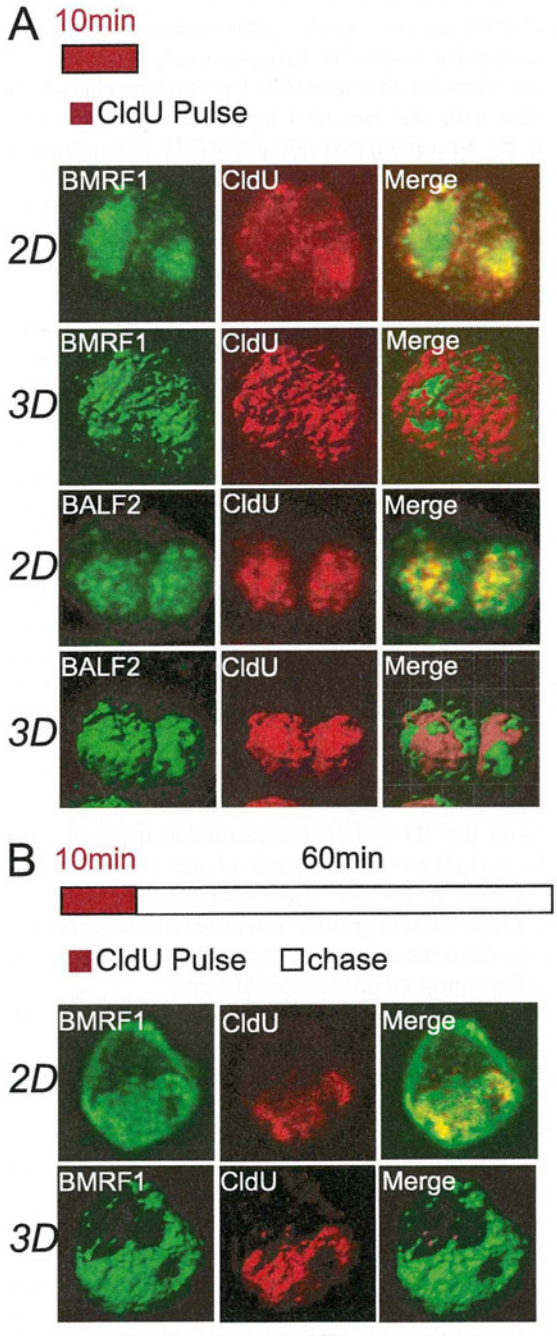

FIG. 3. Newly synthesized viral DNA genomes localized outside the BMRF1 core move to the inside. Pulse-chase labeling experiments were performed with Tet-BZLF1/B95-8 cells at 24 h after induction. Outlines of the experimental protocol are given at the tops of panels A and B. (A) Tet-BZLF1/B95-8 cells were pulse-labeled with CldU for 10 min at 24 h postinduction. (B) The pulse-labeled cells were washed, and then chased for 1 h (B). For the 2D images, cells were treated with 0.5% mCSK buffer and stained with anti-BMRF1 or -BALF2 (green) and anti-CldU (red) antibodies. These images show brightest-point projections of 60 images collected at 0.26-μm steps in the *z* axis. The same data are displayed as 3D topographical reconstructions of the BMRF1 or BALF2 protein and CldU-labeled viral DNA (left and middle panels, respectively). The right panels show 3D surface reconstruction images.

MMR proteins are recruited and loaded inside BMRF1 cores. Next, the spatial localization of mismatch repair (MMR) proteins was determined. As shown in a representative image, the majority of PCNA was localized inside the BMRF1 cores, while some appeared on their surfaces (Fig. 5A). This is in contrast to the localization of HRR factors and MRN complexes (Fig. 4). Regarding the localization of MSH2, MSH3, and MSH6, unlike PCNA, they were almost completely localized inside the BMRF1 cores (Fig. 5B, C, and D). Such a difference in localization implies that MMR factors are last to be loaded onto viral DNAs, whereas the BMRF1 protein and PCNA are first loaded on newly synthesized viral DNA, resulting in enlargement of the BMRF1 core. Because MSH3 and MSH6 interact with PCNA, such loading might trigger transfer of a series of host MMR proteins to sites of viral DNA maturation. Taken together, the results indicate that MMR of the viral DNA genome might occur after BMRF1 proteins bind to a viral DNA and contribute to a mature intact viral genome.

DISCUSSION

Previous cross-sectional studies of EBV replication compartments by confocal laser microscopy demonstrated EBV replication proteins to be localized at viral replication compartments, also revealing variation in staining pattern between individual proteins (9). Here, the BMRF1 protein, which is multifunctional, showed a homogenous, not dot-like, distribution. This is evidence of BMRF1-rich structures (BMRF1 cores) existing within viral replication compartments. Three-dimensional surface reconstruction imaging revealed that replication compartments are partitioned into two subdomains, inside and outside the BMRF1 core. This approach further revealed factories for viral genome synthesis and maturation mediated by HRR and MMR host factors. The BALF5 DNA polymerase and BALF2 ssDNA binding protein were almost colocalized outside the cores. Since both proteins are thought to form an item of the viral elongation machinery acting at replication forks on the replicating EBV genome, they would position at sites of viral genome synthesis. Pulse-chase experiments indicated that viral DNA genomes were synthesized mainly outside BMRF1 cores, where HRR factors were localized, with subsequent movement into the cores. On the other hand, MMR proteins were recruited to viral DNAs exclusively inside, indicating that loading of MMR proteins onto viral DNA is likely to occur at the step of viral genome maturation. These observations let us propose a new model of viral DNA synthesis and maturation as follows. First, viral DNA genomes are synthesized by viral replication machinery, which is coupled with homologous recombination with the help of host HRR factors. Next, BMRF1 proteins bound to the newly synthesized viral DNA are assembled to form cores. During the progression of viral replication, the size of the core increases. Inside, MMR factors are loaded through PCNA to repair and mature newly synthesized viral DNA. The observed sequential loading of HRR factors and MMR proteins on newly synthesized viral DNA implies that spatially and temporarily different repair mechanisms are working during EBV genome maturation.

From our recent resolution of the crystal structure of C-terminally truncated BMRF1 protein (32), the molecular struc-

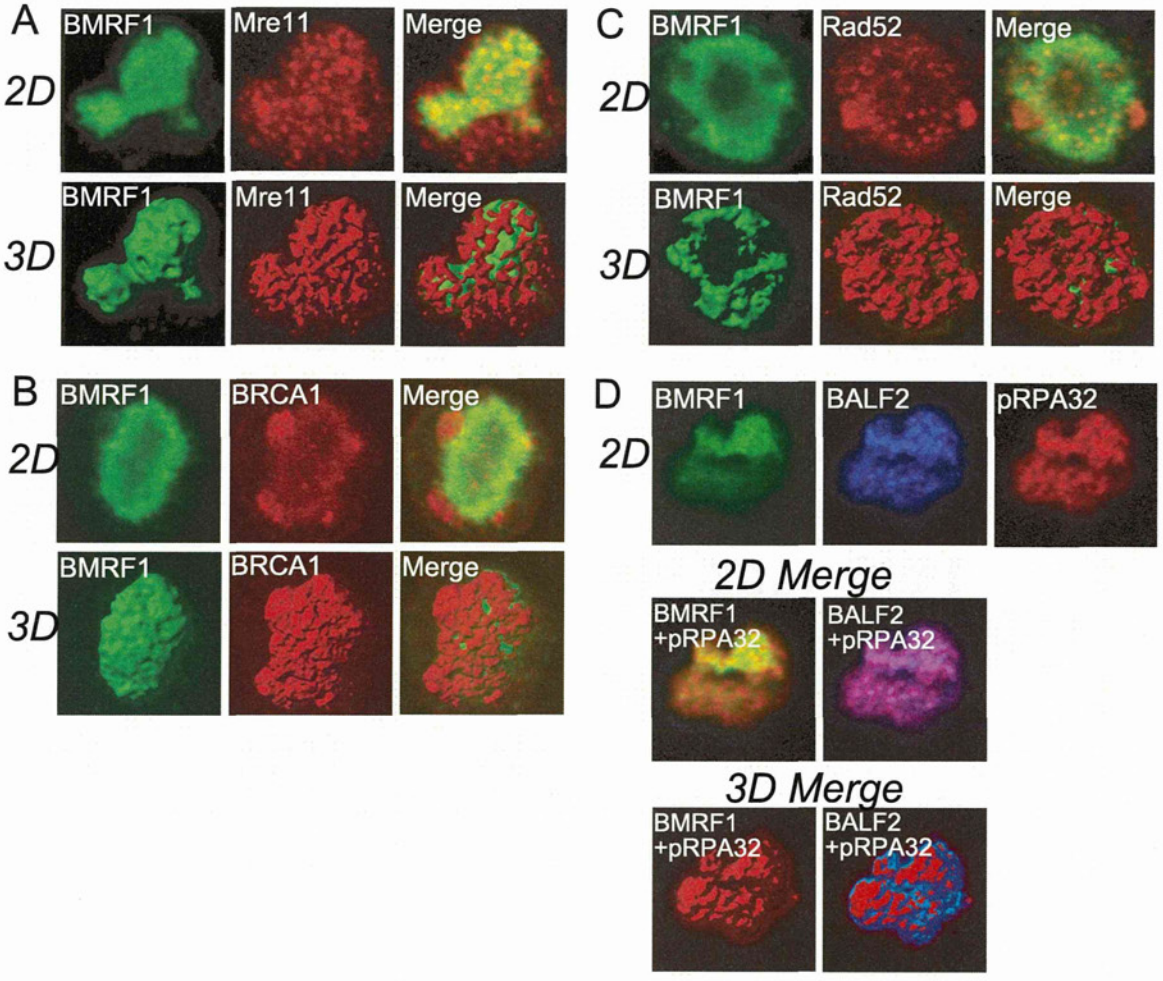

FIG. 4. Homologous recombinational repair proteins are located both outside and inside BMRF1 cores. (A to C) Lytic replication-induced Tet-BZLF1/B95-8 cells were treated with mCSK buffer, fixed with 70% ethanol, and stained with combinations of the indicated antibodies as follows: (A) anti-BMRF1 (green) and anti-Mre11 (red) antibodies; (B) anti-BMRF1 (green) and anti-BRCA1 ser-1524 (red) antibodies; (C) anti-BMRF1 (green) and anti-Rad52 (red) antibodies. The 2D images show brightest-point projections of 60 images collected at 0.26-μm steps in the *z* axis. The same data are displayed as 3D topographical reconstructions of each protein (left and middle panels, respectively). The right panels shows 3D surface reconstruction images of both proteins indicated, showing the BMRF1 core covered by HRR proteins. (D) The cells were stained with anti-BMRF1 (green), anti-BALF2 (blue), and anti-phosphorylated RPA32 Ser-4/Ser-8 (red) antibodies. Top panels, 2D images showing a brightest-point projection of 60 images collected at 0.26-μm steps in the *z* axis. Middle panels, each combination of the merged image of the top panels. Bottom panels, each combination of merged 3D surface reconstruction images.

ture shares structural similarity with other processivity factors, such as HSV-1 UL42, HCMV UL44, and human proliferating cell nuclear antigen (PCNA). Although the crystal structure of BMRF1 indicates an interesting tetramer ring formation, electrophoresis and sedimentation assay suggested that the main component of EBV BMRF1 in solution is a head-to-head dimer. Tail-to-tail association of the dimers forms the ring structure. Replication of a recombinant virus with a point mutation at C206E of BMRF1 (which is expected to impair tail-to-tail contact) is severely restricted (34), although the mutant protein possesses the same *in vitro* biochemical activities as the wild type (32), indicating that its tetrameric ring formation might be essential for EBV replication. PCNA proteins adopt a ring-shaped trimer conformation with the head-to-tail contacts, forming a central channel to accommodate the template DNA (6). The BMRF1 ring-shaped structure (30, 32) is almost twice as large as the previously reported PCNA ring structure. In contrast, HSV-1 UL42 stably exists as a monomer (35), whereas HCMV UL44 forms a head-to-head-contacting C-shaped dimer in the crystal structure (1). The BMRF1 dimer formation overlaps the UL44 dimer. Substitutions of positively charged residues on the concave surface of the BMRF1 C-shaped dimer reduce DNA binding affinity. Furthermore, an amino acid mutation disrupting the dimer formation, C95E, results in no DNA binding (32). Another study of dimerized processivity factor HCMV UL44 also indicates that DNA binding affinity is related to dimer formation (1). Thus, the basic concave surface is very important for DNA binding by the dimerized proteins BMRF1 and UL44. UL44 is consequently thought to bind to DNA like PCNA, which surrounds DNA by ring formation (21). The BMRF1 protein is abundantly expressed in the lytic infected cells and is distributed homogenously, not in a dot-like pattern, within the replication compartments. We speculate that the tetrameric ring form of

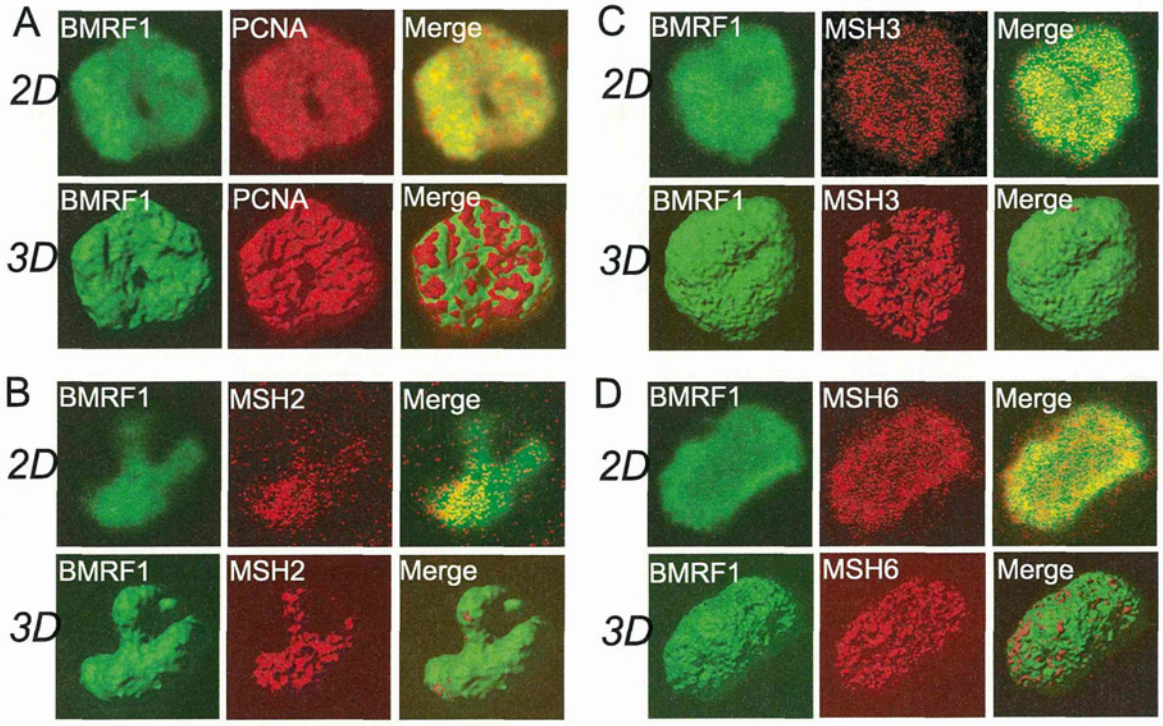

FIG. 5. Mismatch repair proteins such as PCNA, MSH2, MSH3, and MSH6 localize inside BMRF1 cores. Lytic replication-induced Tet-BZLF1/B95-8 cells were treated with mCSK buffer, fixed with 70% ethanol, and stained with combinations of antibodies as follows: (A) anti-BMRF1 (green) and anti-PCNA (red) antibodies; (B) anti-BMRF1 (green) and anti-MSH2 (red) antibodies; (C) anti-BMRF1 (green) and anti-MSH3 (red) antibodies; (D) anti-BMRF1 (green) and anti-MSH6 (red) antibodies. The 2D images show brightest-point projections of 60 images collected at 0.26-μm steps in the z axis. The same data are displayed as a 3D topographical reconstructions of each protein (left and middle panels, respectively). The right panels show 3D surface reconstructions image of both proteins indicated, showing MMR proteins located inside the BMRF1 core.

BMRF1 might be involved in formation of the BMRF1 cores within the replication compartments to protect the synthesized viral DNA by occupying the surfaces of the DNA molecules.

In general, processivity factors are associated with their cognate DNA polymerases on the template during DNA replication. These proteins are also known as "sliding clamps," including PCNA, which interacts with DNA polymerase δ or ε. However, the herpesvirus polymerase processivity factors display different molecular assemblies to cognate viral DNA polymerase. The HSV-1 UL42 form a heterodimer with the UL30 DNA polymerase (35). Mutational analyses of BMRF1 revealed that the monomer form of EBV BMRF1 can function as polymerase processivity factor *in vitro* (32), suggesting that BMRF1 interacts with BALF5 DNA polymerase to form a heterodimer like UL42. Thus, the BMRF1 protein adopts different subunit architecture during the replication process.

HRR is a repair system for double-strand breaks (DSBs), essential for cellular survival in eukaryotes, which relies on several proteins, including Rad-51, -52, and -54, the Mre11/Rad50/Nbs1 (MRN) complex, RPA, and BRCA1/2 (5, 28). First, the MRN complex searches DSBs and generates 3′ ssDNA by removing the 5′ ends of the DSB regions, followed by phosphorylated RPA binding to 3′ ssDNA strands. Rad52, BRCA1, and BRCA2 replace RPA with Rad51. Both Rad51 and Rad52 bind specifically to the terminal region of tailed duplex DNA, the substrate thought to initiate recombination by promoting homologous pairing and strand transfer reactions *in vivo* (12, 16, 38). HRR is also required to repair replication-associated DNA lesions and replication fork stalling or collapse (31, 39). In eukaryotic cells, HRR also occurs coupled with replication at replication forks to ensure proper replication and prevent genomic instability (11). Considering these results and our present study, the host HRR system might be used, being necessary for efficient viral replication coupled with viral genome replication.

It has recently been reported that the HSV-1 alkaline exonuclease UL12 and the single-stranded-DNA binding protein ICP8 interact with each other, are recruited to replication compartments, and together mediate strand exchange *in vitro*, suggesting a role as a two-component recombinase reminiscent of the lambda Red α/β recombination system (3). Further, RPA, Mre11, Rad50, Nbs1, and Rad51 are recruited to HSV-1 replication compartments as in the case of EBV (46). These viral and cellular proteins might together be involved in homologous recombinational repair of herpesvirus genome DNA maturation. However, unlike in the case of EBV (23), there is no induction of hyperphosphorylation of RPA upon productive HSV-1 infection. Instead, endogenous hyperphosphorylated RPA is sequestered away from replication compartments into discrete nuclear foci (VICE domains) that are enriched for cellular components involved in protein folding and degradation (45). Since those authors never observed either induction of RPA hyperphosphorylation or recruitment of phosphorylated RPA to HSV-1 replication compartments, they

concluded that these signaling molecules are excluded from sites that contain viral DNA. Although the discrepancy remains unclear, hyperphosphorylated RPA32, Rad51, Rad52, and MRN complex were recruited to the EBV replication compartments and interacted with EBV genomic DNA (23). HRR represents an error-free subpathway of damage tolerance, allowing replicational bypass of lesions through a template switch. The EBV genome is amplified to several hundred copies during lytic infection, and further, the small interfering RNA (siRNA) depletion of Rad51 or RPA32 reduces new viral DNA synthesis (23). We propose that HRR occurs during EBV lytic genome replication with the aid of host cellular HRR factors and that the HRR factors might help not only to increase the fidelity of viral replication but also to facilitate viral genome replication.

On the other hand, MMR contributes to recognize and repair DNA mismatches that are generated during chromatin DNA replication in eukaryotic cells (20), correcting 99% of such lesions. Because MMR reduces the number of replication-associated errors, defects in MMR increase the spontaneous mutation rate. The MMR machinery works as a postreplication repair near a replication fork. The first step of MMR is that MSH2-MSH6 or MSH2-MSH3 searches for and recognizes a mismatch region through interaction with the β-clamp accessory protein PCNA (14, 18). A MLH1-PMS2 complex is then recruited, and the mismatch region is removed by endonuclease activity of MLH1-PMS2 and exonuclease (Exo1) (17, 25). Thus, this MMR machinery works as a postreplication repair near a replication fork. Our present data show that some MMR proteins contribute to EBV genome maturation after replication. High-copy replication with high fidelity might require the host MMR machinery to repair produced viral genomes.

ACKNOWLEDGMENTS

We thank Ayumi Kudoh (Salk Institute) and Tohru Daikoku (Toyama University) for discussions and Keizo Tomonaga, Yusuke Matsumoto, and Hiroko Omori (Osaka University) and Y. Tanaka (Nagoya University) for technical suggestions.

This work was supported by grants-in-aid for scientific research from the Ministry of Education, Science, Sports, Culture and Technology of Japan (no. 20390137 and 21022055 to T.T.) and partly by the Uehara Memorial Research Fund (to T.T.).

REFERENCES

1. **Appleton, B. A., A. Loregian, D. J. Filman, D. M. Coen, and J. M. Hogle.** 2004. The cytomegalovirus DNA polymerase subunit UL44 forms a C clamp-shaped dimer. Mol. Cell **15:**233–244.
2. **Baer, R., et al.** 1984. DNA sequence and expression of the B95-8 Epstein-Barr virus genome. Nature **310:**207–211.
3. **Balasubramanian, N., P. Bai, G. Buchek, G. Korza, and S. K. Weller.** 2010. Physical interaction between the herpes simplex virus type 1 exonuclease, UL12, and the DNA double-strand break-sensing MRN complex. J. Virol. **84:**12504–12514.
4. **Bataille, D., and A. Epstein.** 1994. Herpes simplex virus replicative concatemers contain L components in inverted orientation. Virology **203:**384–388.
5. **Benson, F. E., P. Baumann, and S. C. West.** 1998. Synergistic actions of Rad51 and Rad52 in recombination and DNA repair. Nature **391:**401–404.
6. **Bruck, I., and M. O'Donnell.** 2001. The ring-type polymerase sliding clamp family. Genome Biol. **2:**REVIEWS3001.
7. **Cho, M. S., G. Milman, and S. D. Hayward.** 1985. A second Epstein-Barr virus early antigen gene in BamHI fragment M encodes a 48- to 50-kilodalton nuclear protein. J. Virol. **56:**860–866.
8. **Clark, A. B., F. Valle, K. Drotschmann, R. K. Gary, and T. A. Kunkel.** 2000. Functional interaction of proliferating cell nuclear antigen with MSH2-MSH6 and MSH2-MSH3 complexes. J. Biol. Chem. **275:**36498–36501.
9. **Daikoku, T., et al.** 2005. Architecture of replication compartments formed during Epstein-Barr virus lytic replication. J. Virol. **79:**3409–3418.
10. **Daikoku, T., et al.** 2006. Postreplicative mismatch repair factors are recruited to Epstein-Barr virus replication compartments. J. Biol. Chem. **281:**11422–11430.
11. **Delacote, F., and B. S. Lopez.** 2008. Importance of the cell cycle phase for the choice of the appropriate DSB repair pathway, for genome stability maintenance: the trans-S double-strand break repair model. Cell Cycle **7:**33–38.
12. **Errico, A., and V. Costanzo.** 2010. Differences in the DNA replication of unicellular eukaryotes and metazoans: known unknowns. EMBO Rep. **11:**270–278.
13. **Fixman, E. D., G. S. Hayward, and S. D. Hayward.** 1995. Replication of Epstein-Barr virus oriLyt: lack of a dedicated virally encoded origin-binding protein and dependence on Zta in cotransfection assays. J. Virol. **69:**2998–3006.
14. **Flores-Rozas, H., D. Clark, and R. D. Kolodner.** 2000. Proliferating cell nuclear antigen and Msh2p-Msh6p interact to form an active mispair recognition complex. Nat. Genet. **26:**375–378.
15. **Fujita, N., et al.** 1999. Purification, characterization, and cDNA structure of isoamylase from developing endosperm of rice. Planta **208:**283–293.
16. **Gottipati, P., and T. Helleday.** 2009. Transcription-associated recombination in eukaryotes: link between transcription, replication and recombination. Mutagenesis **24:**203–210.
17. **Hoeijmakers, J. H.** 2001. Genome maintenance mechanisms for preventing cancer. Nature **411:**366–374.
18. **Jiricny, J.** 2000. Mediating mismatch repair. Nat. Genet. **24:**6–8.
19. **Kleczkowska, H. E., G. Marra, T. Lettieri, and J. Jiricny.** 2001. hMSH3 and hMSH6 interact with PCNA and colocalize with it to replication foci. Genes Dev. **15:**724–736.
20. **Kolodner, R. D., and G. T. Marsischky.** 1999. Eukaryotic DNA mismatch repair. Curr. Opin. Genet. Dev. **9:**89–96.
21. **Komazin-Meredith, G., et al.** 2008. The human cytomegalovirus UL44 C clamp wraps around DNA. Structure **16:**1214–1225.
22. **Kudoh, A., et al.** 2003. Reactivation of lytic replication from B cells latently infected with Epstein-Barr virus occurs with high S-phase cyclin-dependent kinase activity while inhibiting cellular DNA replication. J. Virol. **77:**851–861.
23. **Kudoh, A., et al.** 2009. Homologous recombinational repair factors are recruited and loaded onto the viral DNA genome in Epstein-Barr virus replication compartments. J. Virol. **83:**6641–6651.
24. **Kuzminov, A.** 2001. DNA replication meets genetic exchange: chromosomal damage and its repair by homologous recombination. Proc. Natl. Acad. Sci. U. S. A. **98:**8461–8468.
25. **Li, G. M.** 2008. Mechanisms and functions of DNA mismatch repair. Cell Res. **18:**85–98.
26. **Li, J. S., et al.** 1987. Association of Epstein-Barr virus early antigen diffuse component and virus-specified DNA polymerase activity. J. Virol. **61:**2947–2949.
27. **Lilley, C. E., C. T. Carson, A. R. Muotri, F. H. Gage, and M. D. Weitzman.** 2005. DNA repair proteins affect the lifecycle of herpes simplex virus 1. Proc. Natl. Acad. Sci. U. S. A. **102:**5844–5849.
28. **Lundin, C., et al.** 2002. Different roles for nonhomologous end joining and homologous recombination following replication arrest in mammalian cells. Mol. Cell. Biol. **22:**5869–5878.
29. **Luo, M. H., K. Rosenke, K. Czornak, and E. A. Fortunato.** 2007. Human cytomegalovirus disrupts both ataxia telangiectasia mutated protein (ATM)- and ATM-Rad3-related kinase-mediated DNA damage responses during lytic infection. J. Virol. **81:**1934–1950.
30. **Makhov, A. M., D. Subramanian, E. Holley-Guthrie, S. C. Kenney, and J. D. Griffith.** 2004. The Epstein-Barr virus polymerase accessory factor BMRF1 adopts a ring-shaped structure as visualized by electron microscopy. J. Biol. Chem. **279:**40358–40361.
31. **Michel, B., et al.** 2001. Rescue of arrested replication forks by homologous recombination. Proc. Natl. Acad. Sci. U. S. A. **98:**8181–8188.
32. **Murayama, K., et al.** 2009. Crystal structure of Epstein-Barr virus DNA polymerase processivity factor BMRF1. J. Biol. Chem. **284:**35896–35905.
33. **Nakayama, S., et al.** 2009. Epstein-Barr virus polymerase processivity factor enhances BALF2 promoter transcription as a coactivator for the BZLF1 immediate-early protein. J. Biol. Chem. **284:**21557–21568.
34. **Nakayama, S., et al.** 2010. Tetrameric ring formation of Epstein-Barr virus polymerase processivity factor is crucial for viral replication. J. Virol. **84:**12589–12598.
35. **Randell, J. C., and D. M. Coen.** 2004. The herpes simplex virus processivity factor, UL42, binds DNA as a monomer. J. Mol. Biol. **335:**409–413.
36. **Shirata, N., et al.** 2005. Activation of ataxia telangiectasia-mutated DNA damage checkpoint signal transduction elicited by herpes simplex virus infection. J. Biol. Chem. **280:**30336–30341.
37. **Taylor, T. J., and D. M. Knipe.** 2004. Proteomics of herpes simplex virus replication compartments: association of cellular DNA replication, repair, recombination, and chromatin remodeling proteins with ICP8. J. Virol. **78:**5856–5866.
38. **Thompson, L. H., and J. M. Hinz.** 2009. Cellular and molecular consequences of defective Fanconi anemia proteins in replication-coupled DNA repair: mechanistic insights. Mutat. Res. **668:**54–72.

39. **Toueille, M., and U. Hubscher.** 2004. Regulation of the DNA replication fork: a way to fight genomic instability. Chromosoma **113:**113–125.
40. **Tsurumi, T.** 1993. Purification and characterization of the DNA-binding activity of the Epstein-Barr virus DNA polymerase accessory protein BMRF1 gene products, as expressed in insect cells by using the baculovirus system. J. Virol. **67:**1681–1687.
41. **Tsurumi, T., T. Daikoku, R. Kurachi, and Y. Nishiyama.** 1993. Functional interaction between Epstein-Barr virus DNA polymerase catalytic subunit and its accessory subunit in vitro. J. Virol. **67:**7648–7653.
42. **Tsurumi, T., et al.** 1998. Overexpression, purification and helix-destabilizing properties of Epstein-Barr virus ssDNA-binding protein. J. Gen. Virol. **79:** 1257–1264.
43. **Tsurumi, T., et al.** 1993. Functional expression and characterization of the Epstein-Barr virus DNA polymerase catalytic subunit. J. Virol. **67:**4651–4658.
44. **Weber, P. C., M. D. Challberg, N. J. Nelson, M. Levine, and J. C. Glorioso.** 1988. Inversion events in the HSV-1 genome are directly mediated by the viral DNA replication machinery and lack sequence specificity. Cell **54:**369–381.
45. **Wilkinson, D. E., and S. K. Weller.** 2006. Herpes simplex virus type I disrupts the ATR-dependent DNA-damage response during lytic infection. J. Cell Sci. **119:**2695–2703.
46. **Wilkinson, D. E., and S. K. Weller.** 2004. Recruitment of cellular recombination and repair proteins to sites of herpes simplex virus type 1 DNA replication is dependent on the composition of viral proteins within prereplicative sites and correlates with the induction of the DNA damage response. J. Virol. **78:**4783–4796.
47. **Xie, Y., C. Counter, and E. Alani.** 1999. Characterization of the repeat-tract instability and mutator phenotypes conferred by a Tn3 insertion in RFC1, the large subunit of the yeast clamp loader. Genetics **151:**499–509.
48. **Zhang, Q., et al.** 1996. Functional and physical interactions between the Epstein-Barr virus (EBV) proteins BZLF1 and BMRF1: effects on EBV transcription and lytic replication. J. Virol. **70:**5131–5142.
49. **Zhang, X., S. Efstathiou, and A. Simmons.** 1994. Identification of novel herpes simplex virus replicative intermediates by field inversion gel electrophoresis: implications for viral DNA amplification strategies. Virology **202:** 530–539.

Journal of General Virology (2011), **92**, 2590–2595 DOI 10.1099/vir.0.033712-0

Short Communication

Identification of Epstein–Barr virus-infected CD27$^+$ memory B-cells in liver or stem cell transplant patients

Yoshinori Ito,[1] Shinji Kawabe,[1] Seiji Kojima,[1] Fumihiko Nakamura,[2] Yukihiro Nishiyama,[3] Kenichiro Kaneko,[4] Tetsuya Kiuchi,[5] Hisami Ando[4] and Hiroshi Kimura[2]

Correspondence
Yoshinori Ito
yoshi-i@med.nagoya-u.ac.jp

[1]Department of Pediatrics, Nagoya University Graduate School of Medicine, Nagoya, Japan
[2]Department of Hematology and Oncology, Tenri Hospital, Tenri, Japan
[3]Department of Virology, Nagoya University Graduate School of Medicine, Nagoya, Japan
[4]Department of Pediatric Surgery, Nagoya University Graduate School of Medicine, Nagoya, Japan
[5]Department of Transplant Surgery, Nagoya University Graduate School of Medicine, Nagoya, Japan

To analyse the phenotype of Epstein–Barr virus (EBV)-infected lymphocytes in EBV-associated infections, cells from eight haematopoietic stem cell/liver transplantation recipients with elevated EBV viral loads were examined by a novel quantitative assay designed to identify EBV-infected cells by using a flow cytometric detection of fluorescent *in situ* hybridization (FISH) assay. By this assay, 0.05–0.78 % of peripheral blood lymphocytes tested positive for EBV, and the EBV-infected cells were CD20$^+$ B-cells in all eight patients. Of the CD20$^+$ EBV-infected lymphocytes, 48–83 % of cells tested IgD positive and 49–100 % of cells tested CD27 positive. Additionally, the number of EBV-infected cells assayed by using FISH was significantly correlated with the EBV-DNA load, as determined by real-time PCR (r^2=0.88, P<0.0001). The FISH assay enabled us to characterize EBV-infected cells and perform a quantitative analysis in patients with EBV infection after stem cell/liver transplantation.

Received 8 June 2011
Accepted 29 July 2011

Epstein–Barr virus (EBV) is a ubiquitous virus that infects humans worldwide. Acute infectious mononucleosis (AIM) is the primary EBV infection (Rickinson & Kieff, 2006), and current understanding of primary EBV infection is primarily based on studies of patients with AIM. EBV infects naïve B-cells in the tonsils and activates them; these infected B-cells can differentiate through a germinal centre in lymphoid tissue, becoming resting memory B-cells (Thorley-Lawson & Gross, 2004). Alternatively, EBV may infect memory cells directly (Kurth *et al.*, 2000).

EBV-related post-transplant lymphoproliferative disorder (PTLD) is a life-threatening disease following haematopoietic stem cell or solid organ transplantation, and EBV infects B-lymphocytes in most cases (Rickinson & Kieff, 2006). EBV also causes mild/moderate symptomatic diseases other than PTLD. Recently, serial EBV load monitoring following solid organ transplantation identified a population of recipients who subsequently developed and maintained very high EBV loads in the absence of clinical symptoms (Bingler *et al.*, 2008; D'Antiga *et al.*, 2007; Green *et al.*, 2009). In these cases, EBV also infected B-cells in peripheral blood (Gotoh *et al.*, 2010). Characterizing the EBV-infected lymphocytes in these different EBV-associated infections may provide a better understanding of the pathophysiology of EBV-related disorders.

We recently established a novel quantitative assay to identify EBV-infected cells that uses flow cytometric detection of fluorescent *in situ* hybridization (FISH) (Kimura *et al.*, 2009). With a fluorescein-conjugated probe that specifically hybridizes to the EBV-encoded small RNA (EBER), both nuclear EBER and surface lymphocyte antigens can be stained. This assay can be used with peripheral blood to characterize EBV-infected lymphocytes. With this FISH assay, we analysed peripheral blood in patients with EBV-associated T/NK-cell lymphoproliferative disease. The EBER-positive cells were found to be CD3$^+$CD4$^-$CD8$^-$TCR$\gamma\delta^+$ T-cells in patients with hydroa vacciniforme-like lymphoproliferative disease, which is an EBV-positive cutaneous T-cell lymphoma (Kimura *et al.*, 2009), thus providing new insight into EBV-associated T/NK-cell lymphoproliferative disease.

In this study, we applied the FISH assay to peripheral blood from eight haematopoietic stem cell/liver transplantation recipients with increasing amounts of EBV DNA in their peripheral blood to characterize the EBV-infected lymphocytes. The number of EBER-positive cells in peripheral

blood, as quantified by the FISH assay, was also compared with the EBV-DNA load, as determined by quantitative PCR.

Four haematopoietic stem cell transplant recipients and four liver transplant recipients were enrolled in the study. A quantitative PCR assay detected a large amount of EBV DNA in the peripheral blood of all of the patients. A prospective analysis of EBV load in peripheral blood is routinely performed in our department to provide an early diagnosis of EBV-associated diseases in patients after stem cell and liver transplantation. Blood samples for the FISH assay (described below) were obtained from: four haematopoietic stem cell transplantation recipients with suspected symptomatic EBV infection; four liver transplant recipients without clinical symptoms but with the continuous presence of high EBV viral loads; and five healthy volunteers with a history of EBV infection. PBMCs were separated by density gradients from whole blood. Informed consent was obtained from all participants or their parents. This study was approved by the University of Nagoya Institutional Review Board.

Viral load was examined in the PBMCs of all patients. Viral DNA was extracted from 1×10^6 PBMCs by using QIAamp DNA blood kits (Qiagen). The real-time quantitative PCR assay was performed as previously described (Kimura *et al.*, 1999; Wada *et al.*, 2007). The FISH assay was also performed as previously described (Kimura *et al.*, 2009). Briefly, for surface marker staining, 5×10^5 PBMCs were stained with phycoerythrin cyanin 5 (PC5)-labelled anti-CD20 mAb (clone B-Ly1, DakoCytomation), and phycoerythrin (PE)-labelled anti-IgD mAb (clone IgD26, MACS) or biotin-labelled anti-CD27 (clone O323, Biolegend) mAb, followed by streptavidin–PC5 (eBioscience), for 1 h at 4 °C. The cells were then fixed with 1 % acetic acid in 4 % paraformaldehyde/PBS (pH 7.4) for 40 min at 4 °C. After washing, cells were permeabilized in 50 µl 0.5 % Tween 20/PBS at room temperature. The cells were resuspended in 45 µl of hybridization solution (6 % dextran sulphate, 10 mM NaCl, 17.5 % formamide, 0.061 % sodium pyrophosphate, 0.12 % polyvinylpyrrolidone, 0.12 % Ficoll, 5 mM Na_2EDTA, 50 mM Tris/HCl, pH 7.4) containing 12 nM of the EBER PNA Probe/FITC (Y5200, DakoCytomation). Hybridization was carried out for 1 h at 56 °C. Then, the cells were washed twice and an Alexa Fluor 488 Signal Amplification kit (Molecular Probes) was used to enhance fluorescence and photostability. The stained cells were analysed using a FACSCalibur and CellQuest software (BD Biosciences). Up to 50 000 events were recorded for each analysis. The lymphocytes were gated by standard forward- and side-scatter profiles. Dead cells were not excluded. To determine the lower detection limit of the FISH assay for EBV$^+$ cells, we mixed EBV$^+$ Raji and EBV$^-$ BJAB cells in various ratios and quantified them by using the FISH assay (Kimura *et al.*, 2009). EBER-positive cells could be quantified, as the Raji/BJAB ratio was between 0.1 (EBV-positive cells were 10 %) and 0.0001 (0.01 %), although the population of CD19$^+$EBER$^+$ cells was less clear at a ratio of 0.0001. Therefore, the detection limit of the FISH assay was considered to be 0.01–0.1 %.

Statistical analyses were performed with SPSS for Windows version 18.0 (SPSS). Regression analysis (Pearson product-moment correlation coefficient) was used to compare the FISH assay and the real-time PCR. Values of $P<0.05$ were considered statistically significant.

The characteristics of each patient are shown in Table 1. Based on the FISH assay, EBER-positive lymphocytes were detected in all eight patients and they ranged from 0.05 to 0.78 % of lymphocytes (Table 1). The mean and SEM of the percentage of the EBER-positive cells was 0.27 ± 0.13 % in haematopoietic stem cell transplantation recipients and 0.38 ± 0.15 % in liver transplantation recipients. The phenotypes of each patient are also shown in Table 1. The percentage of the total of CD20$^+$ lymphocytes varies among patients, particularly in patients with haematopoietic stem cell transplant. In contrast, the percentages in the five healthy volunteers were within the normal range (14, 15, 19, 22 and 25). The EBV-infected cells were CD20$^+$IgD$^+$ or CD20$^+$CD27$^+$ cells in most patients. Representative results of the dual staining are shown in Fig. 1. In patient 2, EBER-positive lymphocytes were detected in 6 % of CD20$^+$ lymphocytes, and EBV-infected cells were mostly IgD$^+$ or CD27$^+$ cells. In patient 4, EBER-positive lymphocytes were detected in 2 % of CD20$^+$ lymphocytes, and EBV-infected cells were detected in approximately 50 % of IgD$^+$ or CD27$^+$ cells. The main EBV-infected cells were identified as being CD20$^+$IgD$^+$ or CD20$^+$CD27$^+$ cells in other patients. In contrast, EBER-positive cells were not detected in any of the five healthy volunteers (representative results are also shown in Fig. 1c, d), and the mean percentage of IgD$^+$ cells or CD27$^+$ cells within the sample of CD20$^+$ lymphocytes was 66 % (range, 56–78 %) and 48 % (range, 33–59 %), respectively.

Next, we compared the results of the FISH assay with those from the real-time quantitative PCR. The number of EBER-positive cells assayed by FISH was significantly correlated with the EBV-DNA load determined by real-time PCR ($r^2=0.88$, $P<0.0001$; Fig. 2).

The percentage of the total of CD20$^+$ cells in the five healthy volunteers was within the normal range, suggesting that the FISH assay was well performed. In contrast, these percentages vary among patients, particularly in patients with haematopoietic stem cell transplants (from 10 to 66 %, Table 1). Myeloablative chemotherapy followed by haematopoietic stem cell transplantation is associated with substantial B- and T-cell immunodeficiency for a period of up to several years (Douek *et al.*, 2000; Storek *et al.*, 1993). As the reconstitution of B- and T-cells was not parallel, and this reconstitution is influenced by various factors, such as graft-versus-host disease (Storek *et al.*, 2001), the ratio of these cells may vary in patients for prolonged periods after transplantation.

B-cells play a large role in the humoral immune response. Naïve B-cells proliferate and differentiate to yield memory

Table 1. Characteristics of haematopoietic stem cell/liver transplantation recipients with elevated EBV loads

EBER, EBV-encoded small RNA.

No.	Sex	Age (years)	Transplant	Clinical symptoms	Time post-transplant (months)	Time post testing EBV positive (months)	EBV DNA in PBMCs [copies (μg DNA)$^{-1}$]	$CD20^+$ lymphocytes (% of total)	$EBER^+$ lymphocytes (% of total)	Percentage of $CD20^+EBER^+$ lymphocytes		Percentage of $CD20^+EBER^-$ lymphocytes	
										IgD^+	$CD27^+$	IgD^+	$CD27^+$
1	F	7	Bone marrow	Fever, cough, diarrhoea	1	1	41,175	40	0.63	56	80	2	25
2	F	1	Bone marrow	Fever, diarrhoea, rash	3	1	3,730	15	0.10	83	100	16	40
3	F	6	Bone marrow	Malaise, cough, hilar lymphadenopathy	10	1	2,441	10	0.05	58	100	66	32
4	F	48	Cord blood	Hepatomegaly	37	6	10,500	66	0.28	48	49	8	6
5	M	1	Liver	Asymptomatic	9	8	13,392	29	0.39	81	99	11	23
6	F	2	Liver	Asymptomatic	15	15	4,729	12	0.15	79	99	67	40
7	F	2	Liver	Asymptomatic	15	15	8,302	23	0.19	83	98	64	36
8	M	10	Liver	Asymptomatic	96	96	16,438	36	0.78	68	83	27	20

B-cells and long-lived plasma cells in the course of a T-cell-dependent B-cell response. In humans, memory B-cells have mostly been characterized based on two surrogate markers of antigenic experience, namely the expression of isotype switched or somatically mutated immunoglobulins (Yoshida *et al.*, 2010). Human memory B-cells are predominantly identified by the expression of CD27 (Klein *et al.*, 1998). Mutated immunoglobulin sequences are found almost exclusively in $CD27^+$ B-cells, and CD27 is expressed on B-cells upon their activation (Klein *et al.*, 1998); however, it is absent from most cord-blood B-cells (Agematsu *et al.*, 1997). This may be the reason why the percentage of $CD20^+EBER^+CD27^+$ cells in patient 2 was much lower than that observed for other patients in the present study. Following this criteria, peripheral B-cells from adult blood or secondary lymphoid organs can be separated into 50–60 % naïve $CD27^-$ B-cells and 40–50 % $CD27^+$ memory cells. $CD27^+$ B-cells comprise $IgM^-IgD^-CD27^+$ class-switched cells (40 %) and two subsets (Yoshida *et al.*, 2010) of IgM memory cells: $IgM^+IgD^+CD27^+$ (40 %) and $IgM^+IgD^-CD27^+$ (20 %). In addition, a small fraction of IgD-only $CD27^+$ cells exists (<1 % of B-cells) (Yoshida *et al.*, 2010). Hochberg *et al.* (2004) reported that EBV mostly infected IgD^-CD27^+ B-cells (which appear to be $IgM^-IgD^-CD27^+$ class-switched cells or $IgM^+IgD^-CD27^+$ IgM memory cells) in patients with AIM, and this is the same as in latently EBV-infected cells from healthy carriers (Babcock *et al.*, 1998). In most cases of AIM, EBV-infected cells represented 10–50 % of circulating memory B-cells (Hochberg *et al.*, 2004). In this study, the EBV-infected cells were mostly $CD20^+IgD^+$, which appeared to be $IgM^+IgD^+CD27^+$ IgM memory cells. The phenotype of EBV-infected memory cells may differ in immunocompromised patients after transplantation compared with AIM patients. Alternatively, the composition of memory B-cell subsets in peripheral blood may be different between AIM patients and patients after stem cell/liver transplantation. Interestingly, the percentage of $EBER^+CD20^+CD27^+$ B-cells in patient 4, who underwent cord blood transplantation, was much less than in other patients. Further studies are needed to determine whether this difference leads to different clinical features.

In experiments with human B-lymphocytes, each EBV-infected cell was shown to contain one EBV episome 16 h after EBV infection (Alfieri *et al.*, 1991). With regard to cell lines, human lymphoblastoid X50-7 cells contain approximately five EBV genomes per cell (Arribas *et al.*, 1995). Raji cells, which were established in culture from a Burkitt's lymphoma biopsy, contain 50–60 genome equivalents per cell in latent form (Adams & Lindahl, 1975). By using a FISH assay with a specific probe for the *Bam*HI W region of EBV, Rose *et al.* (2002) measured the number of EBV genomes per infected cell in solid organ transplantation recipients with a persistent EBV load of 8–200 genomes per 10^5 PBMCs (low-load carriers) and with a persistent EBV load of more than 200 genomes per 10^5 PBMCs (high-load carriers). Low-load carriers had virus-infected cells harbouring one or two

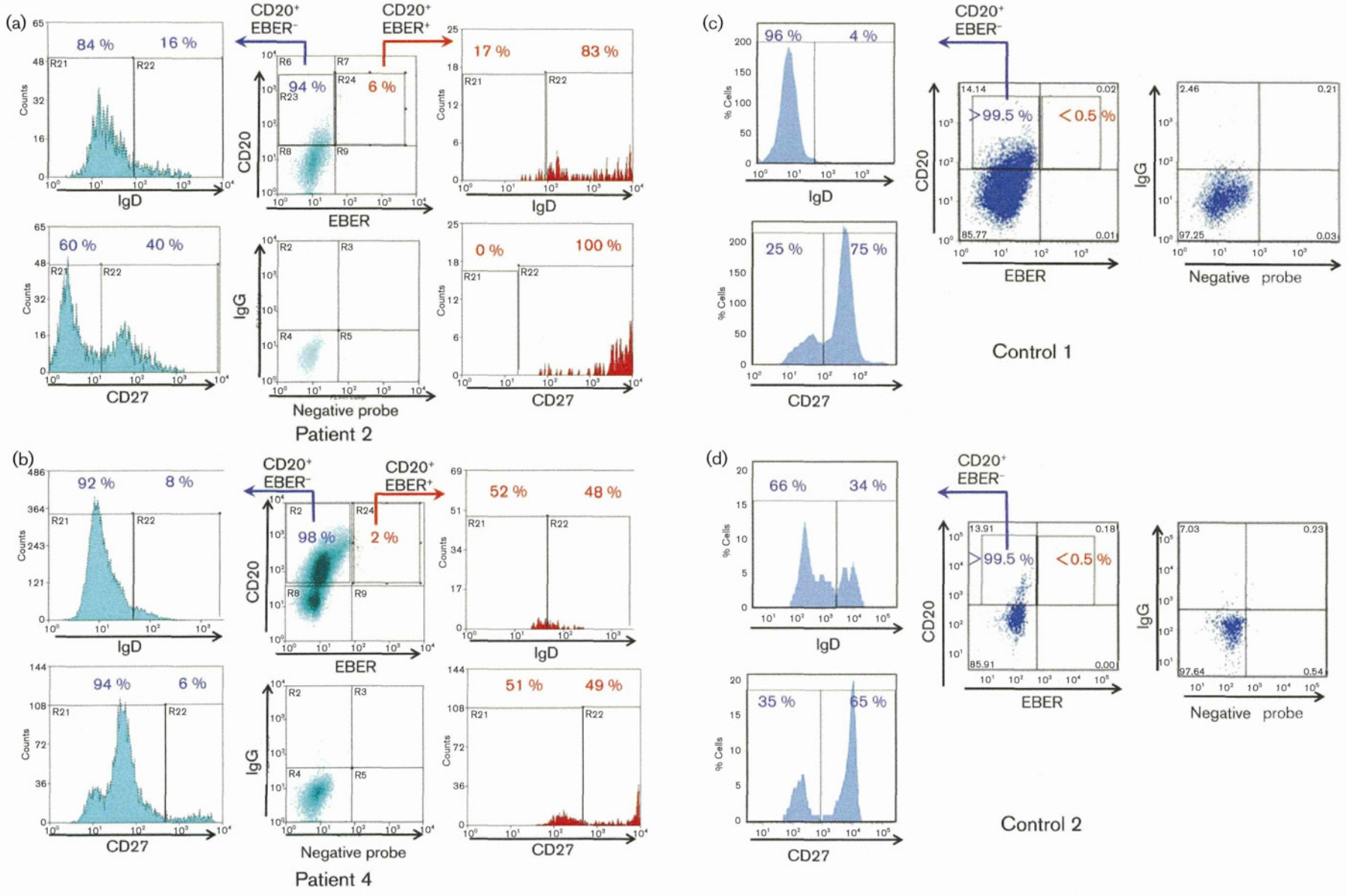

Fig. 1. Characterization of EBV-infected lymphocytes in representative patients. PBMCs were stained with mAbs for surface markers, fixed, permeabilized and hybridized with an EBER probe. The lymphocytes were gated by standard forward- and side-scatter profiles, and plotted on the quadrant that is at the centre of each panel for each patient or control. CD20$^+$EBER$^+$ lymphocytes (red) and CD20$^+$EBER$^-$ lymphocytes (blue) were gated and the expression of IgD or CD27 is shown in each histogram. (a) Patient 2; (b) patient 4; (c) control 1 (a healthy volunteer with a history of EBV infection); (d) control 2.

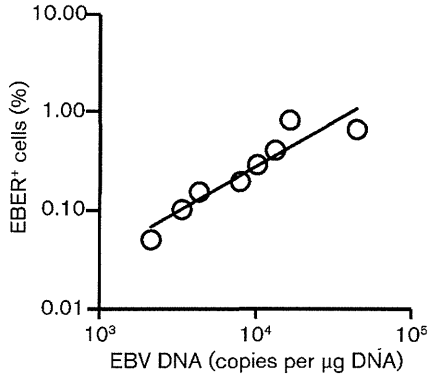

Fig. 2. Correlation between the percentage of EBER-positive lymphocytes, as measured by FISH, and the EBV-DNA load, as measured by using real-time PCR. EBER-positive lymphocytes in PBMCs from all eight patients were analysed by using the FISH assay. Amounts of EBV DNA in PBMCs from all eight patients were measured by using a real-time PCR assay.

genome copies per cell. High-load carriers had two populations of cells; one had one or two genome copies per cell and the other had more than ten copies per cell. By using another FISH assay, Calattini *et al.* (2010) reported that the average number of EBV genomes per cell in B-cells from patients with high EBV-DNA loads ranged from 7.3 to 22.25. EBV was also found at an approximately tenfold lower number of copies in T-cells than in B-cells. In the present study, the number of EBER-positive cells, measured by FISH, was significantly correlated with the EBV-DNA load determined by real-time PCR. As the number of EBERs is not correlated with the number of EBV genomes in infected cells, detection of EBERs does not provide a precise estimate of the number of EBV genomes present per cell. However, the number of EBV-genome equivalents can be calculated if the number of EBV genomes is equal in EBER-positive cells. Looking at the data in Fig. 2, 10^4 copies μg^{-1} of DNA points to the result that the percentage of EBER-positive cells is approximately 0.3 %. Because 1 μg DNA appears to be extracted from 2×10^5 PBMCs (Kimura *et al.*, 1999), 10^4 copies μg^{-1} of DNA is equivalent to 10^4 copies per 2×10^5 PBMCs, that is, five copies per 100 cells. If infected cells represent 0.3 % of cells, 16.7 copies of the EBV genome are in a single infected cell. Additionally, in a separate study we demonstrated a correlation between the number of EBER-positive cells, as measured by FISH, and the amount of EBV DNA in EBV-associated T- or NK-cell lymphoproliferative diseases, in which EBV infects T- or NK cells (unpublished data). The number of EBV genomes was estimated to be one tenth of that observed in the memory B-cells in this study (data not shown). These data are consistent with the results of Calattini *et al.* (2010). Characterizing the phenotype of EBV-infected cells by the FISH assay combined with a real-time PCR assay enables a quantitative analysis of EBV-associated diseases.

Acknowledgements

We thank Shuko Kumagai and Fumiyo Ando for excellent technical support. Potential conflicts of interest: The authors have no commercial or other associations that might pose a conflict of interest. Financial support: Japan Society for the Promotion of Science [Grant-in-Aid for Scientific Research (C) (20591276) to Y. Ito], and Ministry of Health, Labor, and Welfare of Japan [Grant for research on measures for emerging and re-emerging infections (Intractable Infectious Diseases in Organ Transplant Recipients, H21-Shinko-Ippan-009) to H. Kimura.]

References

Adams, A. & Lindahl, T. (1975). Epstein-Barr virus genomes with properties of circular DNA molecules in carrier cells. *Proc Natl Acad Sci U S A* **72**, 1477–1481.

Agematsu, K., Nagumo, H., Yang, F. C., Nakazawa, T., Fukushima, K., Ito, S., Sugita, K., Mori, T., Kobata, T. & other authors (1997). B cell subpopulations separated by CD27 and crucial collaboration of $CD27^+$ B cells and helper T cells in immunoglobulin production. *Eur J Immunol* **27**, 2073–2079.

Alfieri, C., Birkenbach, M. & Kieff, E. (1991). Early events in Epstein-Barr virus infection of human B lymphocytes. *Virology* **181**, 595–608.

Arribas, J. R., Clifford, D. B., Fichtenbaum, C. J., Roberts, R. L., Powderly, W. G. & Storch, G. A. (1995). Detection of Epstein-Barr virus DNA in cerebrospinal fluid for diagnosis of AIDS-related central nervous system lymphoma. *J Clin Microbiol* **33**, 1580–1583.

Babcock, G. J., Decker, L. L., Volk, M. & Thorley-Lawson, D. A. (1998). EBV persistence in memory B cells *in vivo*. *Immunity* **9**, 395–404.

Bingler, M. A., Feingold, B., Miller, S. A., Quivers, E., Michaels, M. G., Green, M., Wadowsky, R. M., Rowe, D. T. & Webber, S. A. (2008). Chronic high Epstein-Barr viral load state and risk for late-onset posttransplant lymphoproliferative disease/lymphoma in children. *Am J Transplant* **8**, 442–445.

Calattini, S., Sereti, I., Scheinberg, P., Kimura, H., Childs, R. W. & Cohen, J. I. (2010). Detection of EBV genomes in plasmablasts/plasma cells and non-B cells in the blood of most patients with EBV lymphoproliferative disorders by using immuno-FISH. *Blood* **116**, 4546–4559.

D'Antiga, L., Del Rizzo, M., Mengoli, C., Cillo, U., Guariso, G. & Zancan, L. (2007). Sustained Epstein–Barr virus detection in paediatric liver transplantation. Insights into the occurrence of late PTLD. *Liver Transpl* **13**, 343–348.

Douek, D. C., Vescio, R. A., Betts, M. R., Brenchley, J. M., Hill, B. J., Zhang, L., Berenson, J. R., Collins, R. H. & Koup, R. A. (2000). Assessment of thymic output in adults after haematopoietic stem-cell transplantation and prediction of T-cell reconstitution. *Lancet* **355**, 1875–1881.

Gotoh, K., Ito, Y., Ohta, R., Iwata, S., Nishiyama, Y., Nakamura, T., Kaneko, K., Kiuchi, T., Ando, H. & Kimura, H. (2010). Immunologic and virologic analyses in pediatric liver transplant recipients with chronic high Epstein–Barr virus loads. *J Infect Dis* **202**, 461–469.

Green, M., Soltys, K., Rowe, D. T., Webber, S. A. & Mazareigos, G. (2009). Chronic high Epstein–Barr viral load carriage in pediatric liver transplant recipients. *Pediatr Transplant* **13**, 319–323.

Hochberg, D., Souza, T., Catalina, M., Sullivan, J. L., Luzuriaga, K. & Thorley-Lawson, D. A. (2004). Acute infection with Epstein-Barr virus targets and overwhelms the peripheral memory B-cell compartment with resting, latently infected cells. *J Virol* **78**, 5194–5204.

Kimura, H., Morita, M., Yabuta, Y., Kuzushima, K., Kato, K., Kojima, S., Matsuyama, T. & Morishima, T. (1999). Quantitative analysis of

Epstein–Barr virus load by using a real-time PCR assay. *J Clin Microbiol* **37**, 132–136.

Kimura, H., Miyake, K., Yamauchi, Y., Nishiyama, K., Iwata, S., Iwatsuki, K., Gotoh, K., Kojima, S., Ito, Y. & Nishiyama, Y. (2009). Identification of Epstein–Barr virus (EBV)-infected lymphocyte subtypes by flow cytometric in situ hybridization in EBV-associated lymphoproliferative diseases. *J Infect Dis* **200**, 1078–1087.

Klein, U., Rajewsky, K. & Küppers, R. (1998). Human immunoglobulin (Ig)M$^+$IgD$^+$ peripheral blood B cells expressing the CD27 cell surface antigen carry somatically mutated variable region genes: CD27 as a general marker for somatically mutated (memory) B cells. *J Exp Med* **188**, 1679–1689.

Kurth, J., Spieker, T., Wustrow, J., Strickler, G. J., Hansmann, L. M., Rajewsky, K. & Küppers, R. (2000). EBV-infected B cells in infectious mononucleosis: viral strategies for spreading in the B cell compartment and establishing latency. *Immunity* **13**, 485–495.

Rickinson, A. B. & Kieff, E. (2006). Epstein-Barr virus. In *Fields Virology*, 5th edn, pp. 2655–2700. Edited by D. M. Knipe & P. M. Howley. Philadelphia, PA: Lippincott Williams & Wilkins.

Rose, C., Green, M., Webber, S., Kingsley, L., Day, R., Watkins, S., Reyes, J. & Rowe, D. (2002). Detection of Epstein–Barr virus genomes in peripheral blood B cells from solid-organ transplant recipients by fluorescence in situ hybridization. *J Clin Microbiol* **40**, 2533–2544.

Storek, J., Ferrara, S., Ku, N., Giorgi, J. V., Champlin, R. E. & Saxon, A. (1993). B cell reconstitution after human bone marrow transplantation: recapitulation of ontogeny? *Bone Marrow Transplant* **12**, 387–398.

Storek, J., Wells, D., Dawson, M. A., Storer, B. & Maloney, D. G. (2001). Factors influencing B lymphopoiesis after allogeneic hematopoietic cell transplantation. *Blood* **98**, 489–491.

Thorley-Lawson, D. A. & Gross, A. (2004). Persistence of the Epstein–Barr virus and the origins of associated lymphomas. *N Engl J Med* **350**, 1328–1337.

Wada, K., Kubota, N., Ito, Y., Yagasaki, H., Kato, K., Yoshikawa, T., Ono, Y., Ando, H., Fujimoto, Y. & other authors (2007). Simultaneous quantification of Epstein–Barr virus, cytomegalovirus, and human herpesvirus 6 DNA in samples from transplant recipients by multiplex real-time PCR assay. *J Clin Microbiol* **45**, 1426–1432.

Yoshida, T., Mei, H., Dörner, T., Hiepe, F., Radbruch, A., Fillatreau, S. & Hoyer, B. F. (2010). Memory B and memory plasma cells. *Immunol Rev* **237**, 117–139.

Journal of Clinical Virology 50 (2011) 244–246

Contents lists available at ScienceDirect

Journal of Clinical Virology

journal homepage: www.elsevier.com/locate/jcv

Short communication

Kinetics of Epstein-Barr virus load and virus-specific CD8+ T cells in acute infectious mononucleosis

Yo Hoshino[a], Kazuo Nishikawa[b], Yoshinori Ito[a], Kiyotaka Kuzushima[c], Hiroshi Kimura[d,*]

[a] Department of Pediatrics, Nagoya University Graduate School of Medicine, Japan
[b] Department of Pediatrics, Nagoya Ekisaikai Hospital, Japan
[c] Division of Immunology, Aichi Cancer Center Research Institute, Nagoya, Japan
[d] Department of Virology, Nagoya University Graduate School of Medicine, 65 Tsurumai-Cho, Showa-Ku, Nagoya 466-8550, Japan

ARTICLE INFO

Article history:
Received 20 October 2010
Received in revised form
24 November 2010
Accepted 25 November 2010

Keywords:
Epstein-Barr virus
Infectious mononucleosis
CTL
Viral load
EBV-specific CD8+ T cells

ABSTRACT

Background: During the convalescent phase of acute infectious mononucleosis (AIM), Epstein-Barr virus (EBV) load shrinks rapidly in association with a rapid decline in the number of EBV-specific CD8+ T cells. The actual contribution of EBV-specific CD8+ T cells in reducing EBV load, however, is not known.
Objectives: To clarify the impact of EBV-specific CD8+ T cells on the contraction of EBV load in AIM, we estimated half-lives of both EBV load and EBV-specific CD8+ T cells.
Study design: Blood was serially taken from five pediatric patients with AIM during the convalescent period, including the very early phase, and both EBV load and EBV-specific CD8+ T cell numbers were assayed.
Results: EBV load declined rapidly (half-life 1.5 d) during the first 2 weeks after onset of symptoms. This half-life was seven-fold shorter than that reported for CD27+ memory B cells. Subsequently, the EBV load declined much more slowly, with a half-life of 38.7 d. EBV-specific CD8+ T cell numbers also declined concomitantly with the decrease in EBV load. The half-life of EBV-specific CD8+ T cells during first 2 weeks was 2.9 d. The number of EBV-specific CD8+ T cells and the rate of change of viral load correlated significantly ($R^2 \geq 0.8$; $p \leq 0.02$).
Conclusions: The short half-life of EBV load, together with the strong correlation between the number of EBV-specific CD8+ T cells and the rate of change of viral load indicates an active role for EBV-specific CD8+ T cells in elimination of EBV in AIM.

1. Background

Epstein-Barr virus (EBV) is a ubiquitous viral pathogen that causes acute infectious mononucleosis (AIM) and various malignant diseases, such as Burkitt's lymphoma, nasal NK/T lymphoma, nasopharyngeal carcinoma, and post-transplant lymphoproliferative disorders, in both immunocompromised and immunocompetent hosts.[1] EBV-specific CD8+ T cells play important roles in the control of EBV in these diseases.[2] During the convalescent phase of AIM, the EBV load shrinks rapidly in association with a rapid decline in the number of EBV-specific CD8+ T cells, itself caused by activation-induced cell death.[3] However, the extent to which EBV-specific CD8+ T cells contribute to the decline in EBV load in peripheral blood mononuclear cells remains unknown.

2. Objectives

To clarify the impact of EBV-specific CD8+ T cells on the decline in EBV load, we estimated the half-lives of EBV load and EBV-specific CD8+ T cells during the convalescent period of AIM and also evaluated the correlation between them.

3. Study design

Blood samples were serially obtained from five pediatric patients with AIM after written informed consent had been obtained from their parents. AIM was diagnosed by clinical findings and serological examinations, as previously described.[4] Their ages ranged from 5 to 14 years (median, 9 years). The first samples were obtained within the first week of onset of AIM symptoms. Peripheral blood mononuclear cells were separated, frozen, and stored until required. EBV load in peripheral blood mononuclear cells was measured by real-time PCR and expressed as copies/microgram DNA.[4,5] EBV-specific CD8+ T cells were enumerated by intracellular interferon-γ assay against autologous lymphoblastoid cell lines by

Abbreviations: EBV, Epstein-Barr virus; AIM, acute infectious mononucleosis.

* Corresponding author. Tel.: +81 52 744 2207; fax: +81 52 744 2452.
E-mail address: hkimura@med.nagoya-u.ac.jp (H. Kimura).

1386-6532/$ – see front matter © 2010 Elsevier B.V. All rights reserved.
doi:10.1016/j.jcv.2010.11.017

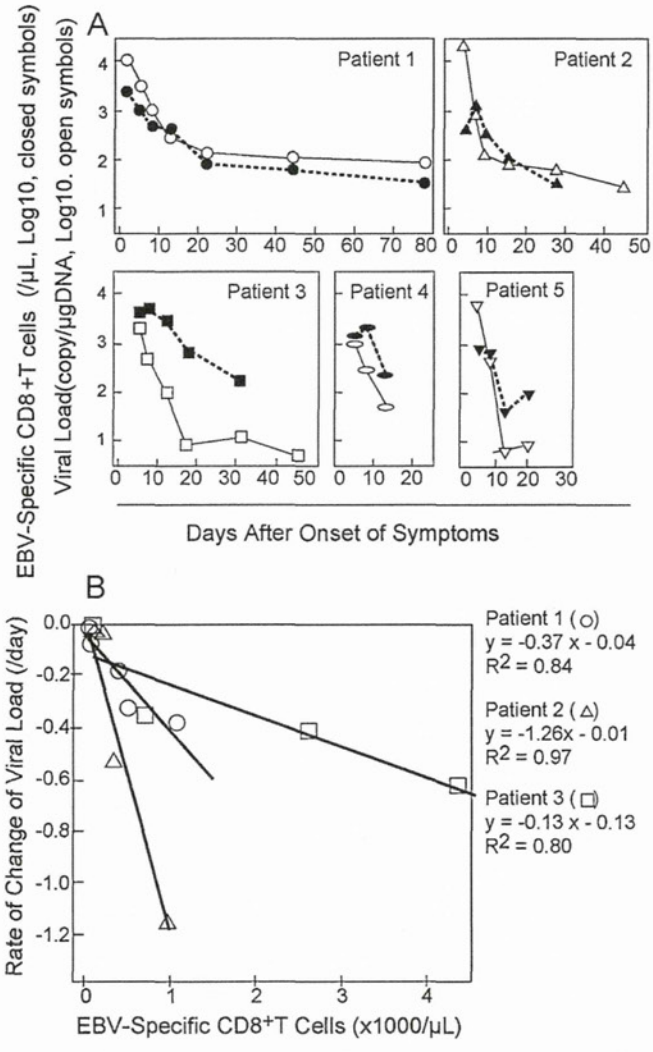

Fig. 1. Kinetics of Epstein-Barr virus (EBV) load and EBV-specific CD8⁺ T cells in patients with acute infectious mononucleosis. (A) EBV vial load was measured by real-time PCR (open symbols connected with solid lines), and EBV-specific CD8⁺ T cell counts by intracellular interferon-γ assay against autologous lymphoblastoid cell lines and flow cytometry (closed symbols connected with broken lines). (B) Correlation between EBV-specific CD8⁺ T cell counts and rate of change in EBV load was estimated by linear regression analysis. Approximations of the rate of change were calculated from three data points. Using v_1, v_2, and v_3, which are the natural logarithms of viral loads at t_1, t_2, and t_3, respectively, the following equation was used to calculate the rate of change of viral load for a unit of viral load at $t=t_2$: $dv/dt_{(t=t2)} = (x_2 - x_1)(t_3 - t_2)/(t_2 - t_1)(t_3 - t_1) + (x_3 - x_2)(t_2 - t_1)/(t_3 - t_2)(t_3 - t_1)$. Solid lines indicate linear regression curves for patients 1, 2, and 3, from whom sufficient data points were obtained.

flow cytometry.[3,6]

4. Results

First, we analyzed the kinetics of EBV load and number of EBV-specific CD8⁺ T cells. EBV load was highest at the time of first sampling (2–6 d after onset) in all patients and decreased thereafter (Fig. 1A). Peak viral loads were $10^{4.1}$, $10^{4.3}$, $10^{3.3}$, $10^{3.0}$, and $10^{3.8}$ per μg DNA in patients 1, 2, 3, 4, and 5, respectively. EBV viral loads declined rapidly during the first 1–2 weeks after onset and more slowly thereafter (Fig. 1A). The mean estimated half-life of EBV load during the early convalescent period (~2 weeks after onset) was 1.5 ± 0.2 d (Table 1); this is seven-fold shorter than that reported for CD27⁺ memory B cells (11.1 d).[7] EBV infection in the peripheral blood of AIM patients is restricted to CD27⁺ memory B cells.[8] The mean estimated half-life of EBV load after the 2 weeks was 38.7 ± 15.0. In contrast, number of EBV-specific CD8⁺ T cells increased slightly in three of the five patients and then declined (Fig. 1A). In the remaining patients, the number of EBV-specific CD8⁺ T cells peaked at the time of their first visit ($10^{3.5}$ and $10^{2.9}$ per μL blood in patients 1 and 5, respectively). Number of EBV-specific CD8⁺ T cells declined almost parallel with viral load (half-life 2.9 ± 0.4 d) during the early convalescent period (Table 1).

Table 1
Half-lives of Epstein-Barr virus (EBV) load and EBV-specific CD8⁺ T cells in patients with acute infectious mononucleosis.

Patient	Half-life of EBV load (days)		Half-life of EBV-specific CD8⁺ T cells in acute phase (days) (within 2 weeks of onset)
	Acute phase (within 2 weeks of onset)	Convalescent phase (after 2 weeks of onset)	
1	2.2	22.6	3.8
2	1.5	24.9	2.9
3	1.6	68.7	3.8
4	1.6	n.a.	2.5
5	0.7	n.a.	1.6
Mean ± SE	1.5 ± 0.2	38.7 ± 15.0	2.9 ± 0.4

The shorter half-life of EBV load compared with normal memory B cells suggests the presence of a mechanism that actively removes EBV from blood, such as cytotoxic immune effecter cells. We hypothesized that EBV-specific CD8⁺ T cells play an important role in clearing EBV from blood. EBV load may decrease at a rate proportional to the number of EBV-specific CD8⁺ T cells. To prove this hypothesis, we transformed the time-series of EBV load data into rate of change and examined the correlation between the number of EBV-specific CD8⁺ T cells and the rate of change in viral load. Because multiple data points were necessary for regression analysis, three of the five patients (1, 2, and 3) were analyzed. As shown in Fig. 1B, the analysis revealed a significant positive linear correlation between the rate of change in viral load and the number of EBV-specific CD8⁺ T cells ($R^2 \geq 0.8$, $p \leq 0.02$).

5. Discussion

To clarify the impact of EBV-specific CD8⁺ T cells on the decline in EBV load, we estimated the half-lives of both EBV load and EBV-specific CD8⁺ T cells during the very early phase of the convalescent period of AIM using intervals as short as 2 d. We also evaluated the correlation between the EBV load and the number of EBV-specific CD8⁺ T cells. Our data indicate that during the very early period of AIM, the half-life of EBV load is shorter than that of normal memory B cells and that the rate of change in EBV load was correlated with the number of EBV-specific CD8⁺ T cells in a linear manner. These results suggest that EBV-specific CD8⁺ T cells actively contribute to the decline in EBV load.

Recently, Hadinoto *et al.* reported that linear exponential decay of latent EBV load with a half-life of 7.5 ± 3.7 d was found in patients with AIM during the 30–50 d after the first clinic visit.[9] Due to its similarity to the reported half-life of memory B cells (11.1 d),[7] the authors proposed a model of exponential decay of EBV-infected cells by simple homeostasis of memory B cells, suggesting a passive role for cell-mediated immunity. Hadinoto's paper did not specify the interval between the onset of symptoms and the first clinic visit, and the intervals between assays seemed to be around 1 week. It is possible that EBV-specific CD8⁺ T cells play an important role in the control of EBV load during an earlier stage of AIM. In the very early phase of AIM, EBV infects naïve B cells that express full sets of latent EBV genes.[2] These naïve B cells are either eliminated by EBV-specific CTL or differentiate into memory B cells. In the second phase, the EBV-infected memory B cells express only

restricted kinds of EBV genes,[2] which may help with evasion from EBV-specific CD8+ cells. In the present study, we obtained 2–3 samples per week from the very early period of acute-phase AIM. Thus, the more frequent samples taken at an earlier stage of disease may be the reason for the disagreement in EBV load half-life. In fact, if samples are taken only once per week, a half-life shorter than 3 days will not be detected in two weeks or less.

During the acute phase of AIM, viral loads decreased, even in blood taken only 2 d after symptom onset. Interestingly, we observed a transient increase in EBV-specific CD8+ T cells in three patients; this may be due to a programmed proliferation of T cells.[10–12] In studies in mice, the decrease in pathogen-specific CD8+ T cells is programmed and independent of antigen loads (programmed contraction).[13,14] This is in agreement with current concepts of antigen-driven expansion and contraction of CD8+ T cells during acute infection.[3] A recent paper proposed the model of EBV dynamics in post-transplant lymphoproliferative disorders.[15] The model estimates both doubling times and half-lives of EBV in various situations under the antiviral agents, Rituximab, or adoptive immunotherapy with or without taking into account episomal or lytic origins.

In conclusion, the shorter half-life of EBV load together with the strong correlation between EBV-specific CD8+ T cell numbers and the rate of change of viral load suggests an active role for EBV-specific CD8+ T cells in the elimination of EBV. Further investigations of the interaction between EBV and EBV-specific CD8+ T cells during the period of increasing viral load will be necessary to understand the dynamic interaction between EBV and the immune system during AIM.

Conflict of interest statement

All authors state that they have no conflicts of interest that could inappropriately influence this work.

Acknowledgements

We thank Drs. Jeffrey I. Cohen and Kennichi C. Dowdell at Laboratory of Clinical Infectious Diseases, NIAID, for advice and suggestions. This study was supported by a grant from the Ministry of Education, Culture, Sports, Science and Technology of Japan (13670793).

References

1. Cohen JI. Epstein-Barr virus infection. *N Engl J Med* 2000;**343**(7):481–92.
2. Hislop AD, Taylor GS, Sauce D, Rickinson AB. Cellular responses to viral infection in humans: lessons from Epstein-Barr virus. *Annu Rev Immunol* 2007;**25**:587–617.
3. Hoshino Y, Morishima T, Kimura H, Nishikawa K, Tsurumi T, Kuzushima K. Antigen-driven expansion and contraction of CD8+-activated T cells in primary EBV infection. *J Immunol* 1999;**163**(10):5735–40.
4. Kimura H, Morita M, Yabuta Y, Kuzushima K, Kato K, Kojima S, et al. Quantitative analysis of Epstein-Barr virus load by using a real-time PCR assay. *J Clin Microbiol* 1999;**37**(1):132–6.
5. Hoshino Y, Kimura H, Tanaka N, Tsuge I, Kudo K, Horibe K, et al. Prospective monitoring of the Epstein-Barr virus DNA by a real-time quantitative polymerase chain reaction after allogenic stem cell transplantation. *Br J Haematol* 2001;**115**(1):105–11.
6. Kuzushima K, Kimura H, Hoshino Y, Yoshimi A, Tsuge I, Horibe K, et al. Longitudinal dynamics of Epstein-Barr virus-specific cytotoxic T lymphocytes during posttransplant lymphoproliferative disorder. *J Infect Dis* 2000;**182**(3):937–40.
7. Macallan DC, Wallace DL, Zhang Y, Ghattas H, Asquith B, de Lara C, et al. B-cell kinetics in humans: rapid turnover of peripheral blood memory cells. *Blood* 2005;**105**(9):3633–40.
8. Hochberg D, Souza T, Catalina M, Sullivan JL, Luzuriaga K, Thorley-Lawson DA. Acute infection with Epstein-Barr virus targets and overwhelms the peripheral memory B-cell compartment with resting: latently infected cells. *J Virol* 2004;**78**(10):5194–204.
9. Hadinoto V, Shapiro M, Greenough TC, Sullivan JL, Luzuriaga K, Thorley-Lawson DA. On the dynamics of acute EBV infection and the pathogenesis of infectious mononucleosis. *Blood* 2008;**111**(3):1420–7.
10. Kaech SM, Ahmed R. Memory CD8+ T cell differentiation: initial antigen encounter triggers a developmental program in naive cells. *Nat Immunol* 2001;**2**(5):415–22.
11. van Stipdonk MJ, Lemmens EE, Schoenberger SP. Naive CTLs require a single brief period of antigenic stimulation for clonal expansion and differentiation. *Nat Immunol* 2001;**2**(5):423–9.
12. van Stipdonk MJ, Hardenberg G, Bijker MS, Lemmens EE, Droin NM, Green DR, et al. Dynamic programming of CD8+ T lymphocyte responses. *Nat Immunol* 2003;**4**(4):361–5.
13. Badovinac VP, Porter BB, Harty JT. Programmed contraction of CD8(+) T cells after infection. *Nat Immunol* 2002;**3**(7):619–26.
14. Badovinac VP, Harty JT. Programming, demarcating, and manipulating CD8+ T-cell memory. *Immunol Rev* 2006;**211**:67–80.
15. Funk GA, Gosert R, Hirsch HH. Viral dynamics in transplant patients: implications for disease. *Lancet Infect Dis* 2007;**7**(7):460–72.

UICC
global cancer control

IJC
International Journal of Cancer

Bortezomib induces apoptosis in T lymphoma cells and natural killer lymphoma cells independent of Epstein-Barr virus infection

Seiko Iwata[1], Shoko Yano[1], Yoshinori Ito[2], Yoko Ushijima[1], Kensei Gotoh[2], Jun-ichi Kawada[3], Shigeyoshi Fujiwara[4], Koichi Sugimoto[5], Yasushi Isobe[5], Yukihiro Nishiyama[1] and Hiroshi Kimura[1]

[1] Department of Virology, Nagoya University Graduate School of Medicine, Nagoya, Japan
[2] Department of Pediatrics, Nagoya University Graduate School of Medicine, Nagoya, Japan
[3] Department of Infection and Immunology, Aichi Children's Health and Medical Center, Aichi, Japan
[4] Department of Infectious Diseases, National Research Institute for Child Health and Development, Tokyo, Japan
[5] Department of Hematology, Juntendo University School of Medicine, Tokyo, Japan

Epstein-Barr virus (EBV), which infects not only B cells, but also T cells and natural killer (NK) cells, is associated with multiple lymphoid malignancies. Recently, the proteasome inhibitor bortezomib was reported to induce apoptosis of EBV-transformed B cells. We evaluated the killing effect of this proteasome inhibitor on EBV-associated T lymphoma cells and NK lymphoma cells. First, we found that bortezomib treatment decreased the viability of multiple T and NK cell lines. No significant difference was observed between EBV-positive and EBV-negative cell lines. The decreased viability in response to bortezomib treatment was abrogated by a pan-caspase inhibitor. The induction of apoptosis was confirmed by flow cytometric assessment of annexin V staining. Additionally, cleavage of caspases and polyadenosine diphosphate-ribose polymerase, increased expression of phosphorylated IκB, and decreased expression of inhibitor of apoptotic proteins were detected by immunoblotting in bortezomib-treated cell lines. We found that bortezomib induced lytic infection in EBV-positive T cell lines, although the existence of EBV did not modulate the killing effect of bortezomib. Finally, we administered bortezomib to peripheral blood mononuclear cells from five patients with EBV-associated lymphoproliferative diseases. Bortezomib had a greater killing effect on EBV-infected cells. These results indicate that bortezomib killed T or NK lymphoma cells by inducing apoptosis, regardless of the presence or absence of EBV.

Key words: Epstein-Barr virus, proteasome inhibitor, apoptosis, lytic infection, NF-κB

Abbreviations: 7-AAD: 7-aminoactinomycin D; BARTs: *Bam*HI-A rightward transcripts; cIAP: cellular IAP; DMSO: dimethyl sulfoxide; EBV: Epstein-Barr virus; EBER: EBV-encoded small RNA; EBNA: EBV nuclear antigen; FISH: Flow cytometric in situ hybridization; IAPs: inhibitors of apoptotic proteins; LMP: latent membrane protein; LCL: lymphoblastoid cell line; MNCs: mononuclear cells; NK: natural killer; NF-κB: nuclear factor-κB; PBS: phosphate-buffered saline; PE: phycoerythrin; PARP: polyadenosine diphosphate-ribose polymerase; RT: reverse transcription; SDS: sodium dodecyl sulfate; XIAP: X-linked IAP; β2m: β2-microglobulin

Grant sponsor: Ministry of Education, Culture, Sports, Science and Technology, Japan; **Grant number:** H21-Nanchi-094; **Grant sponsor:** Ministry of Health, Labor, and Welfare of Japan (Health and Labour Science Research Grant on intractable diseases)
DOI: 10.1002/ijc.25873
History: Received 17 Jun 2010; Accepted 30 Nov 2010; Online 17 Dec 2010

Correspondence to: Hiroshi Kimura, Department of Virology, Nagoya University Graduate School of Medicine, 65 Tsurumai-cho, Showa-ku, Nagoya 466-8550, Japan, Tel.: +81-52-744-2451
Fax: +81-52-744-2452, E-mail: hkimura@med.nagoya-u.ac.jp

The ubiquitous Epstein-Barr virus (EBV) infects most individuals by early adulthood and typically remains latent throughout life. EBV not only infects B cells but also T cells and natural killer (NK) cells and has been associated with multiple lymphoid malignancies such as Burkitt lymphoma, diffuse large B cell lymphoma, Hodgkin lymphoma, post-transplant lymphoproliferative disorders, nasal NK/T lymphoma, hydroa vacciniforme-like lymphoma, aggressive NK cell leukemia, and chronic active EBV infection.[1–4] EBV plays an important role in the pathogenesis of many of these malignancies through its ability to establish latent infection and induce the proliferation of infected cells.[5] Some of these EBV-associated lymphoid malignancies are refractory and resistant to conventional chemotherapies. Rituximab, a humanized monoclonal antibody against CD20, targets B cell-specific surface antigens present on EBV-transformed malignant cells. Currently, Rituximab is used in the treatment and prophylaxis of B cell lymphoma and lymphoproliferative disorders.[6,7] However, a continuing need exists for effective treatments of T and NK cell lymphoid malignancies, and novel approaches of molecular target therapy are desirable.

Recently, bortezomib was reported to induce apoptosis in EBV-transformed B cells and prolong survival of mice inoculated with EBV-transformed B cells.[8] Bortezomib is an inhibitor of the 26S proteasome.[9] Proteasomes are multi-protein

complexes that degrade ubiquitinated proteins, including those involved in cell cycle regulation, oncogenesis, and apoptosis. Inhibition of the proteasome can result in apoptosis in malignant cells.[10,11] Bortezomib is approved for the treatment of multiple myeloma and is in clinical trials for non-Hodgkin lymphoma, prostate cancer, and lung cancer.[12,13] A key factor in the ability of bortezomib to kill myeloma cells is that it blocks the activation of nuclear factor-κB (NF-κB).[14] In normal cells, NF-κB is bound to the inhibitory protein IκB, which maintains it in an inactive form in the cytoplasm. Once activated, NF-κB can then enter the nucleus and initiate many actions in the tumor cell that help the cell to survive and proliferate. As a result of inhibiting the proteasome and thus the activation of NF-κB, bortezomib may induce apoptosis by reducing the expression of inflammatory molecules and cell adhesion molecules.[14] Additionally, a study has reported that bortezomib can lead to EBV lytic infection.[15] In EBV-infected lymphocytes, only a few viral genes are expressed to maintain latency and to avoid host immune mechanisms.[1,5] Bortezomib may alter the pattern of viral gene expression thus converting a latent infection to a lytic infection.

In our study, we evaluated the killing effect of bortezomib on EBV-associated T/NK lymphoma cells. To investigate the mechanism of killing, we administered bortezomib to multiple EBV-positive and -negative T and NK cell lines. We further administered bortezomib *ex vivo* to lymphoma cells from patients with EBV-associated lymphoid malignancies.

Material and Methods

Cell lines and reagents

Raji, a latency type III cell line, is an EBV-positive B cell line derived from Burkitt lymphoma.[16] Lymphoblastoid cell line (LCL)-1 and LCL-2, latency type III cell lines, are EBV-positive B cell lines transformed with B95-8 EBV from peripheral blood B lymphocytes. BJAB is an EBV-negative B cell line. SNT-13 and SNT-16[17] are EBV-positive T cell lines. SNK-6[17] and KAI-3[18] are EBV-positive NK cell lines. SNT-13, -16, SNK-6, and KAI-3 were derived from patients with chronic active EBV infection or nasal NK/T cell lymphomas. Jurkat[19] and KHYG-1[20] are EBV-negative T and NK cell lines, respectively. Jurkat was derived from a patient with acute T lymphoblastic leukemia. KHYG-1 was derived from a patient with aggressive NK cell leukemia.

MT-2 cell line was established from cord mononuclear cells by co-culture with adult T cell leukemia cells, and harbors human T cell-leukemia virus type I.[21] MT-2/rEBV/9-7 cell line was established by infection of MT-2 cells with the hygromycin-resistant B95-8 strain.[22] MT-2/hyg cell line, transfected with a hygromycin-resistant gene, and MT-2/rEBV/9-7 were used to verify the difference of EBV presence in the T cell lines. Similarly, NKL cell line[23] was derived from a patient with NK cell leukemia, and TL1 cell line[24] was established from NKL cells infected with Akata-transfected recombinant EBV strain containing a neomycin-resistant gene. TL1 and NKL were used to verify the difference of EBV presence in the NK cell lines.

Raji, LCL-1, LCL-2, BJAB, and Jurkat cells were grown in RPMI 1640 supplemented with 10% heat-inactivated fetal bovine serum, penicillin, and streptomycin (complete media). The medium for SNT-13, -16, KAI3, SNK-6, KHYG1, TL1, and NKL was complete media supplemented with 100 U/ml human interleukin-2. The medium for MT-2/hyg and MT-2/rEBV/9-7 was complete media supplemented with 0.2 mg/ml hygromycin. TL1 underwent periodic selection with G418.

Bortezomib, a gift from Millennium Pharmaceuticals (Cambridge, MA), was dissolved in phosphate-buffered saline (PBS). The pan-caspase inhibitor Q-VD-OPH (Calbiochem, La Jolla, CA) and the proteasome inhibitor MG132 (Biomol International, Plymouth Meeting, PA) were dissolved in dimethyl sulfoxide (DMSO).

Cell viability and apoptosis assays

Cells (2×10^5/ml) were cultured in 24-well plates and cell viability was quantified by trypan blue exclusion. The pan-caspase inhibitor Q-VD-OPH (50 μM) was added at 1 hr prior to the addition of bortezomib. These experiments were performed in duplicate and the results are shown as the mean of two wells.

Apoptosis was measured by flow cytometry using an annexin V-phycoerythrin (PE)/7-aminoactinomycin D (7-AAD) apoptosis assay kit (BD Pharmingen Biosciences, San Diego, CA) according to the manufacturer's protocol. Briefly, 2×10^5 cells were treated with various concentrations of bortezomib for 6 hr, washed with ice-cold PBS, resuspended in binding buffer, incubated with annexin V-PE and 7-AAD for 15 min, and then analyzed by flow cytometry. Viable cells were defined as those negative for annexin V-PE and 7-AAD staining, and early apoptotic cells were defined as those positive for annexin V-PE and negative for 7-AAD staining. Stained cells were analyzed using a FACSCalibur and CellQuest software (Becton Dickinson, Franklin Lakes, NJ).

Immunoblots

Whole-cell extracts were lysed directly with sodium dodecyl sulfate (SDS) sample buffer (50 mM Tris-HCl, pH 6.8, 2% SDS, 10% glycerol, 6% 2-mercaptoethanol, 0.0025% bromophenol blue). Cell lysates were separated by SDS-polyacrylamide gel electrophoresis and transferred to polyvinylidene difluoride membranes (Immobilon-P membrane; Millipore), and immunoblotted with antibodies. Antibodies were directed against caspase-3, cleaved caspase-3, caspase-9, phosphorylated IκBα, and polyadenosine diphosphate-ribose polymerase (PARP) (Cell Signaling Technology, Beverly, MA); β-actin (Sigma, St. Louis, MO); XIAP and cIAP-2 (R&D Systems, Minneapolis, MN); and p53 (BD Pharmingen Biosciences). To compare the amounts of each protein, densitometoric analysis was performed using ImageJ software ver. 1.43 (NIH, Bethesda, MD).

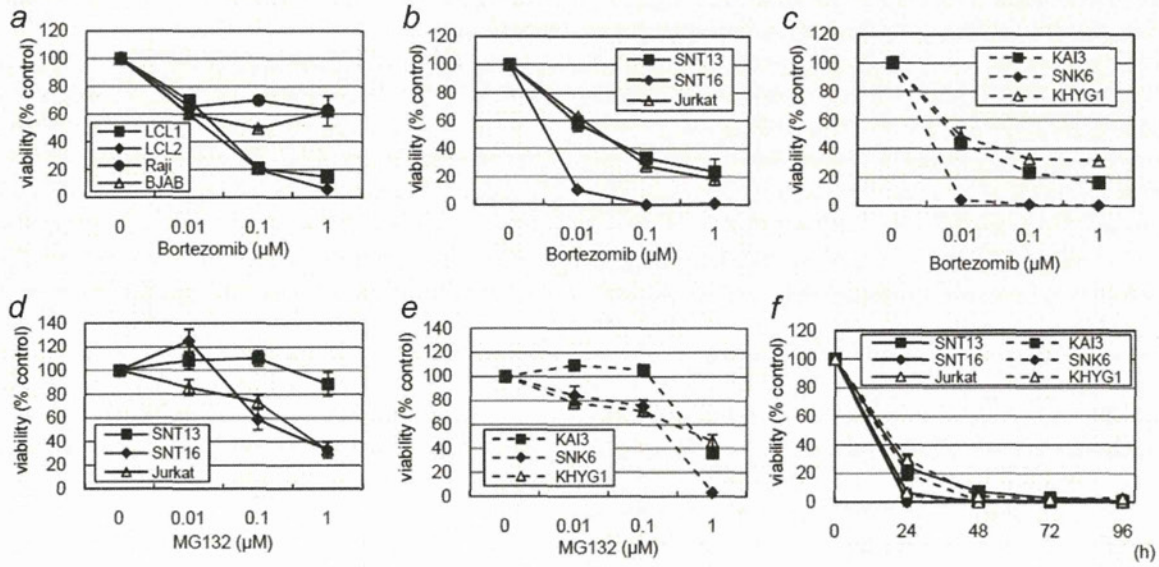

Figure 1. Bortezomib decreases the viability of B, T and NK cell lines. (*a*) B cell lines (Raji, LCL-1, LCL-2, BJAB), (*b*) T cell lines (SNT-13, SNT-16, Jurkat), and (*c*) NK cell lines (KAI-3, SNK-6, KHYG-1) were treated with bortezomib at the indicated concentrations for 24 hr. (*d*) T cell lines or (*e*) NK cell lines were treated with MG132 at various concentrations for 24 hr. (*f*) T or NK cell lines were treated with 1 μM bortezomib for 4 days and viability was determined every 24 hr. The filled markers represent EBV-positive cell lines and the open markers represent EBV-negative cell lines. Viability was calculated as the percentage of viable cells in bortezomib-treated cells *versus* PBS-treated cells. Bars indicate standard errors.

Real-time RT-PCR assay

RNA was extracted from 1×10^6 cells using the QIAmp RNeasy Mini Kit (Qiagen, Hilden, Germany). Contaminating DNA was removed by on-column deoxyribonuclease digestion using the RNase-Free DNase Set (Qiagen). Viral mRNA expression was quantified by a one-step multiplex real-time reverse transcription (RT)-PCR using a Mx3000P real-time PCR system (Stratagene, La Jolla, CA), as described previously.[25,26] The stably expressed housekeeping gene β2-microglobulin (β2m) was used as an endogenous control and reference gene for relative quantification.[27] Each experiment was conducted in triplicate and results are shown as the mean of three samples with standard errors. The Mann-Whitney *U*-test was used to compare the expression levels. p values <0.05 were deemed to be statistically significant.

Patients

Peripheral blood mononuclear cells (MNCs) were collected from five patients with EBV-associated diseases. None of these patients had received any immunosuppressive treatment such as steroid therapy or chemotherapy. Patients T-1 (7-year-old boy), T-2 (6-year-old girl), and T-3 (12-year-old boy) had hydroa vacciniforme-like lymphoma, a newly classified EBV-associated T cell lymphoma.[2] In these patients, 10∼20% of the MNCs were infected with EBV, and the EBV-infected cells were primarily γδT cells.[28] The other two patients, Patients NK-1 (14-year-old boy) and NK-2 (9-year-old boy), had chronic active EBV infection, NK cell type.[29–31] In these patients, ∼40% of MNCs were infected with EBV, and the EBV-infected cells were NK cells. MNCs from three healthy donors were used as controls. Informed consent was obtained from all participants or their guardians. Our study was approved by the institutional review board of Nagoya University Hospital.

MNCs were isolated using Ficoll-Paque (Amersham Pharmacia Biotech AB, Uppsala, Sweden) gradient centrifugation. Cells (2×10^5/ml) were cultured in RPMI 1640 supplemented with 10% heat-inactivated fetal bovine serum. For the cell viability study, each experiment was performed in duplicate, and the results are shown as the mean of two wells.

Magnetic cell sorting

The primarily infected cell fractions were separated by magnetic sorting with a TCRγ/δ$^+$ T Cell Isolation Kit or CD56 Microbeads (Miltenyi Biotec, Bergisch Gladbach, Germany). Briefly, cells were magnetically labeled with MicroBeads and separated on a column placed in the MACS separator. The flow-through was collected as a negative fraction depleted of the labeled cells. The magnetically retained cells were flushed out as the positive fraction. The respective purity and recovery rates were 98.3% and 80.0% with the TCRγ/δ $^+$ T Cell Isolation Kit, and 96.4% and 80.9% with CD56 Microbeads.

Flow cytometric in situ hybridization (FISH) assay

To verify that the sorted fraction contained EBV-infected cells, a FISH assay was used.[28] Briefly, cells were fixed with 1% acetic acid/4% paraformaldehyde, permeabilized with 0.5% Tween 20/PBS, and hybridized with a fluorescein-labeled

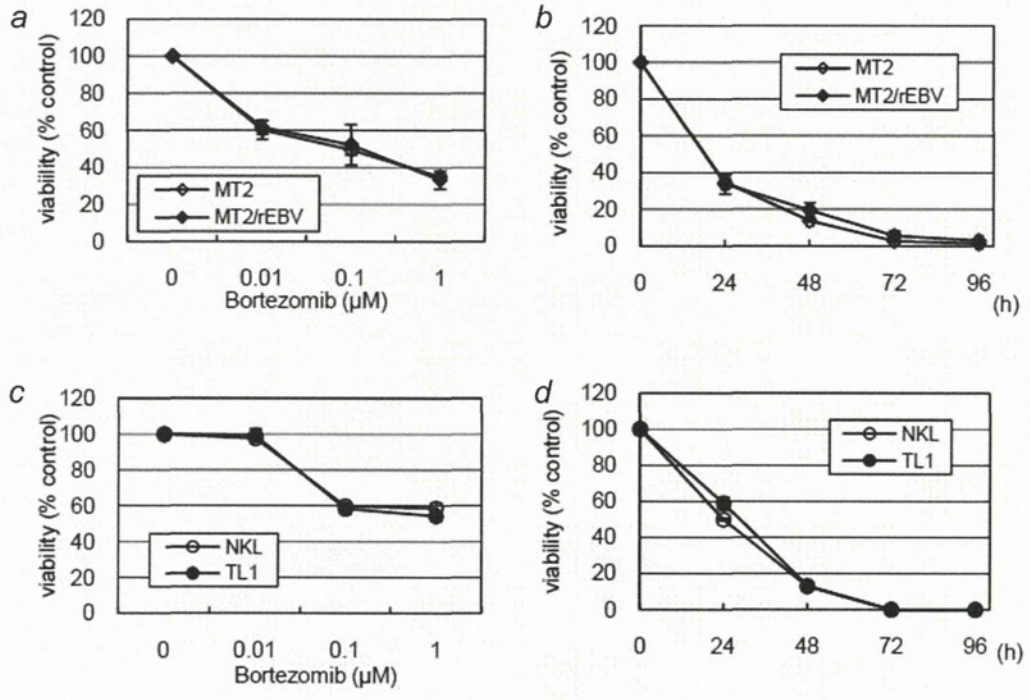

Figure 2. Bortezomib induces similar effects in EBV-positive and -negative cell lines. An EBV-positive T cell line (MT-2/rEBV) and a control cell line (MT/hyg) were treated with various concentrations of bortezomib for 24 hr (*a*) and 1 μM bortezomib for 4 days (*b*). EBV-positive NK cell line (TL1) and its parental line (NKL) were treated with various concentrations of bortezomib for 24 hr (*c*) and 1 μM bortezomib for 4 days (*d*). Bars indicate standard errors.

EBV-encoded small RNA (EBER)-specific peptide nucleic acid probe (Y5200; Dako, Glostrup, Denmark). The fluorescence intensity was enhanced using the AlexaFluor 488 Signal Amplification Kit (Molecular Probes, Eugene, OR), and stained cells were analyzed using a FACSCalibur and CellQuest software (Becton Dickinson).

Results

Bortezomib decreased the viability of B, T and NK cell lines

First, we administered bortezomib to B, T and NK cell lines for 24 hr and counted viable cells. Bortezomib decreased the viability of all four B cell lines: three EBV-positive cell lines (Raji, LCL-1, and LCL-2) and one EBV-negative cell line (BJAB) (Fig. 1*a*). LCL-1 and LCL-2 were more sensitive to bortezomib than Raji or BJAB, consistent with the results of a previous study reporting that bortezomib killed both EBV-positive and -negative B cell lines, but more efficiently in LCLs.[8] Next, we administered bortezomib to T cell lines (SNT-13, SNT-16, Jurkat) and NK cell lines (KAI-3, SNK-6, KHYG-1). Bortezomib decreased the viability of all six target cell lines in a dose-dependent manner (Figs. 1*b* and 1*c*). SNT-16 and SNK-6 seemed to be more sensitive to bortezomib than other cell lines. MG132, another proteasome inhibitor, had less effect on these cell lines (Figs. 1*d* and 1*e*). We administered 1 μM bortezomib to these cell lines for 4 days and determined their viability every 24 hr. We found that bortezomib decreased the viability of these six cell lines by less than 10% at 48 hr or later (Fig. 1*f*). There were no obvious differences on the effect of bortezomib between the EBV-positive and -negative cell lines. Furthermore, to directly compare the effect of bortezomib between EBV-positive and -negative cell lines, we administered bortezomib to MT-2/hyg and MT-2/rEBV/9-7 (Figs. 2*a* and 2*b*), and NKL and TL1 (Figs. 2*c* and 2*d*). We found that bortezomib had almost equal effects on the two cell lines.

Bortezomib induces apoptosis in T and NK cell lines

The induction of apoptosis was confirmed by flow cytometry with annexin V and 7-AAD staining. Bortezomib decreased viable cells, defined as those negative for both annexin V-PE and 7-AAD staining, and increased early apoptotic cells, defined as those positive for annexin V-PE and negative for 7-AAD staining in the four cell lines (Fig. 3*a*): EBV-positive (SNT-16) and EBV-negative T cell lines (Jurkat); and EBV-positive (KAI-3) and EBV-negative NK cell lines (KHYG-1). This result showed that bortezomib induced apoptosis in both T and NK cell lines.

Next, to analyze the mechanism of bortezomib-induced apoptosis, cleavages of caspase and PARP were investigated by immunoblotting. Bortezomib induced cleavage of caspase-3, caspase-9, and PARP in all four cell lines (Fig. 3*b*). The decrease in viability caused by bortezomib was inhibited by pretreatment with Q-VD-OPH, a pan-caspase inhibitor (Fig. 3*c*).

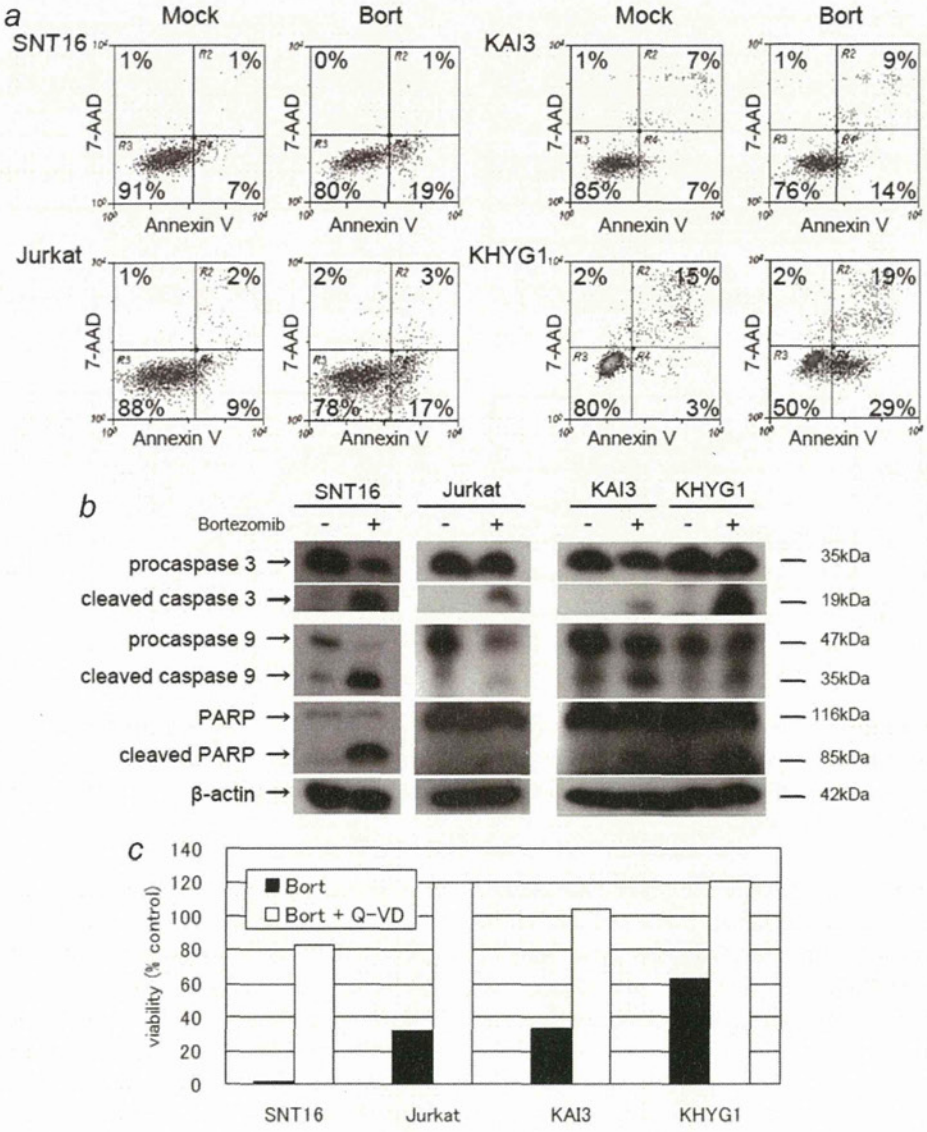

Figure 3. Bortezomib induces apoptosis in T/NK cell lines. (*a*) T cell lines (EBV-positive SNT-16 and -negative Jurkat) and NK cell lines (EBV-positive KAI-3 and -negative KHYG-1) were treated with 1 μM bortezomib for 6 hr. Viable cells were defined as those negative for annexin V-PE and 7-AAD staining, and early apoptotic cells were defined as those positive for annexin V-PE and negative for 7-AAD staining. (*b*) Bortezomib induces cleavage of caspase-3, caspase-9, and PARP. T/NK cell lines were treated with 1 μM bortezomib for 6 hr. Protein lysates were prepared and immunoblotting was performed. β-actin was used as a loading control. Each experiment was performed at least twice. (*c*) Q-VD-OPH inhibits the decrease in viability induced by bortezomib. The pan-caspase inhibitor Q-VD-OPH (50 μM) was added 1 hr prior to the addition of 1 μM bortezomib for 24 hr. Viability was calculated as the percentage of viable cells to PBS-treated cells as assessed by trypan blue exclusion.

Bortezomib blocks activation of NF-κB by inhibiting the proteasome, reducing antiapoptotic factors

In myeloma cells, bortezomib blocks the activation of NF-κB through increasing phosphorylation of IκB.[14] Thus, we confirmed the increase in phosphorylated IκB, which should have been degraded in proteasomes, in bortezomib-treated cell lines by immunoblotting (Fig. 4*a*). Furthermore, we evaluated the effect of bortezomib on two inhibitors of apoptotic proteins (IAPs). Bortezomib down-regulated cellular IAP (cIAP)-2 and X-linked IAP (XIAP) in bortezomib-treated T/NK cell lines (Fig. 4*b*). Densitometoric analysis was performed to confirm that cIAP-2 and XIAP were decreased in all bortezomib-treated cells (Fig. 4*c*). Additionally, bortezomib up-regulated p53, facilitating apoptosis, in some cell lines (Fig. 4*b*).

Bortezomib induces lytic infection of EBV in T cell lines

Next, we analyzed the expression of eight viral genes using a real-time RT-PCR assay: two lytic genes, BZLF1 and gp350/

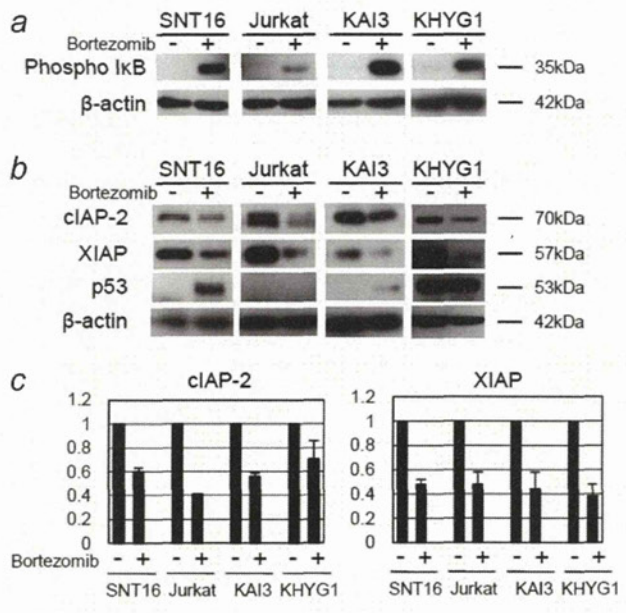

Figure 4. Bortezomib increases phosphorylated IκB and down-regulates the inhibitor of apoptotic proteins in T/NK cell lines. T cell lines (EBV-positive SNT-16 and -negative Jurkat) and NK cell lines (EBV-positive KAI-3 and -negative KHYG-1) were treated with 1 μM bortezomib for 2 hr (*a*) or 8 hr (*b*). Protein lysates were prepared and immunoblotting was performed. β-actin was used as a loading control. Each experiment was performed at least twice. (*c*) Densitometoric analysis was performed using ImageJ software. The data were calculated as the ratios of cIAP-2 (left) and XIAP (right) to β-actin, and the value of PBS-treated cells was assigned as 1. Boxes indicate the mean of two experiments and bars indicate the standard errors.

220; and six latent genes, EBV nuclear antigen (EBNA) 1, EBNA2, latent membrane protein (LMP) 1, LMP2, EBER1, and *Bam*HI-A rightward transcripts (BARTs). We found that the expression of two lytic genes, an immediate early gene (BZLF1) and a late gene (gp350/220), were increased in bortezomib-treated T cell lines (SNT-13 and SNT-16 in Fig. 5). In NK cell lines, however, no such effect was observed. Regarding latent genes, expression of LMP2 was increased in T cell lines. The expressions of other latent genes (EBNA1, EBNA2, LMP1, EBER1, and BARTs) were not obviously different between bortezomib-treated cells and controls (Fig. 5).

Bortezomib decreases the viability of EBV-infected cells from patients with EBV-associated lymphoma

Finally, we investigated the *ex vivo* effect of bortezomib in MNCs from five patients with EBV-associated malignancies. We separated γδT cells and other MNCs from three patients (Patients T-1, T-2, and T-3) with hydroa vacciniforme-like lymphoma by magnetic sorting. Bortezomib (0.5 μM) was administered to each sample of cells, and the viable cells were counted for 3 days. Bortezomib had a greater killing effect on γδT cells that were primarily infected with EBV than on the other MNCs (Fig. 6*a*). Next, we separated the NK cells and other MNCs from two patients (Patients NK-1, and NK-2) with chronic active EBV infection, NK cell-type, and evaluated the effect of bortezomib. For Patient NK-1, experiments were performed twice on different visits. Bortezomib had a greater killing effect on NK cells than on the other MNCs (Fig. 6*b*). In the γδT cell or NK-cell fraction, the absolute number of control viable cells was stable or increased slightly, while the number was clearly decreased with bortezomib treatment (data not shown). Next, we collected blood samples from three healthy donors, sorted the γδT cells, NK cells, and other MNCs, and evaluated their viability with bortezomib treatment. The viability of the cells treated with bortezomib for 3 days was around 100%, indicating that bortezomib did not affect nontumor cells (Fig. 6*c*).

To confirm that the sorted fractions contained EBV-infected cells, EBER-positive cells were quantified using a FISH assay. In Patient T-1 with hydroa vacciniforme-like lymphoma, 19.8% of the MNCs were EBER-positive. After magnetic sorting, 54.7% of γδT cells and 3.8% of the other MNCs were EBER-positive (Fig. 6*d*). To determine whether EBV-infected cells survive selectively, we quantified EBV-positive cells using the FISH assay after bortezomib treatment, and compared the results with PBS-treated control cells. After 3 days, the percentage of EBER-positive bortezomib-treated γδT cells decreased (4.0%), as compared to PBS-treated γδT cells (47.8%) (Fig. 6*e*). Similarly, the percentage of EBER-positive cells in bortezomib-treated NK cells decreased (0.5%), as compared to PBS-treated NK cells (34.1%) (Fig. 6*e*). These results indicate that EBV-positive cells in the control groups survived, while most EBV-positive bortezomib-treated γδT and NK cells died. Moreover, this killing effect was confirmed by flow cytometry using annexin V and 7-AAD staining in Patient NK-1 (Fig. 6*f*).

Discussion

Bortezomib, which is used in the treatment of myeloma, has also been assessed for a variety of other malignancies. In recent studies, this proteasome inhibitor was reported to induce apoptosis in NK lymphoma/leukemia cells,[32,33] and has been tested in cutaneous T cell lymphomas and aggressive T/NK cell lymphomas, including EBV-associated ones.[34,35] Although promising data have accumulated, these trials were small and must be considered preliminary. Furthermore, experience with EBV-associated cases is limited. To our knowledge, there have been no *in vitro* studies to compare the efficacy of bortezomib between EBV-positive and EBV-negative T/ NK lymphoma cells.

In our study, we treated T and NK cell lines with bortezomib to investigate this proteasome inhibitor's ability to induce apoptosis in T and NK lymphoma cells. Bortezomib markedly decreased the viability of T and NK cell lines by inducing apoptosis. Consistent with previous reports, the cleavage of caspases and PARP, increased phosphorylated IκB, and the decreased inhibitor apoptotic proteins indicated